AlphaAdam:Asynchronous Masked Optimization with Dynamic Alpha for Selective Updates

Da Chang [1 2] **Yu Li** [3] **Ganzhao Yuan** [2]

Abstract

In the training of large language models (LLMs), updating parameters more efficiently and stably has always been an important challenge. To achieve efficient parameter updates, existing methods usually achieve performance comparable to full parameter updates through methods such as low-dimensional decomposition or layer-wise selective updates. In this work, we propose AlphaAdam, an optimization framework for LLM from the perspective of intra-layer parameter updates. By decoupling parameter updates and dynamically adjusting their strength, AlphaAdam accelerates convergence and improves training stability. We construct parameter masks based on the consistency of historical momentum and gradient direction and combine them with an adaptive mask strength strategy to ensure efficient optimization and theoretical convergence guarantees, which is also applicable to most momentum-based optimizers. Extensive experiments show that AlphaAdam outperforms state-of-the-art methods such as AdamW in terms of convergence speed and computational efficiency across tasks, including GPT-2 pre-trained and fine-tuned RoBERTa and Llama-7B. Our AlphaAdam implements an optimizer enhancement framework for LLMs through intra-layer asynchronous masked adaptive updates. Our code is available in this link.

1. Introduction

Recent studies have revealed that learning during Large Language Model (LLM) training exhibits low-rank properties, suggesting that learning predominantly occurs in low-dimensional spaces (Gur-Ari et al., 2018; Larsen et al., 2021). This observation has catalyzed the development of methods such as Galore and LDAdam (Zhao et al., 2024; Robert et al., 2024), which achieve comparable performance to full gradient updates while reducing memory consumption through gradient low-rank decomposition. Although low-rank properties do not directly imply sparsity, this insight into optimization in low-dimensional spaces provides crucial understanding for selective parameter updates.

Building on this foundation, several innovative layer-wise selective update methods have emerged, including AutoFreeze, LOMO, LISA, and BAdam (Liu et al., 2021; Lv et al., 2023b; Pan et al., 2024; Luo et al., 2024). These approaches demonstrate performance comparable to or surpassing full-parameter updates by strategically freezing certain layers while updating others. However, existing research has primarily concentrated on layer-level selective adjustments, with limited exploration of selective updates within layers, which leads us to address a fundamental question:

Do we really need to update every parameter within a model layer? How can we systematically determine which parameters need to be updated or left unchanged?

CAdam (Liang et al., 2024), a pioneering work, introduced a masked momentum-based optimization strategy and rigorously established its convergence within a continuous-time optimization framework. By implementing a mask mapping mechanism, this approach enabled selective parameter updates while guaranteeing convergence, opening new avenues in deep learning optimization theory. However, it primarily addressed synchronous masked updates, whereas asynchronous behavior between gradients and momentum is a common phenomenon in practical optimization scenarios.

From a physics perspective, momentum can be conceptualized as the cumulative trend of gradients, analogous to inertia in physical systems. This asynchronicity fundamentally reflects the relationship between current gradients and historical accumulation patterns. Motivated by this observation, we propose an extended theoretical framework that considers masked strategies in asynchronous scenarios and rigorously analyzes their optimization properties.

Through comprehensive theoretical analysis, we demon-

[1]Shenzhen Institutes of Advanced Technology, Shenzhen, China [2]Peng Cheng Laboratory, Shenzhen, China [3]Wuhan university, Hongyi College, Wuhan, China. Correspondence to: Da Chang <changda24@mails.ucas.ac.cn>.

Preprint.

strate that the effectiveness of asynchronous masked strategies is fundamentally linked to two key factors: Gradient Covariance (GC) and Directional Similarity (DS) (Pan, 2023). Our theoretical results reveal that asynchronous masking not only enhances GC but also modulates DS under appropriate conditions, enabling more efficient and stable optimization. Based on these insights, we propose a dynamic mask strength strategy, termed the α-strategy, which optimizes the balance between optimization efficiency and stability through adaptive adjustment of the mask ratio.

Our theoretical analysis bridges the critical gap between gradient-momentum asynchronicity and optimization performance, providing a robust foundation for parameter-level selective updates in deep learning. Through careful examination of the relationships between parameter updates and optimization dynamics, we establish theoretical guarantees for the convergence of our proposed method under practical scenarios.

Extensive experiments demonstrate that our proposed method achieves comparable or superior performance to full parameter updates across various tasks and model scales while significantly improving training stability. Our primary contributions include:

- We develop a theoretical framework for analyzing asynchronous masked updates, providing new perspectives on deep learning optimization;
- We reveal the theoretical mechanisms underlying the superiority of asynchronous masking over synchronous masking, addressing a critical gap in parameter-level selective update strategies;
- We develop a practical dynamic mask strength strategy(α-strategy) that provides efficient implementation while ensuring theoretical convergence.

2. Related Work

2.1. Efficient Training Methods Based on Low-Rank Properties

In LLM training, gradients typically exhibit low-rank characteristics (Gur-Ari et al., 2018; Larsen et al., 2021), and various methods enhance training efficiency and reduce memory usage through techniques like low-rank adaptation, quantization, and block coordinate optimization. Adafactor substantially reduces memory requirements through low-rank decomposition of Adam's second-order moments (Shazeer & Stern, 2018), while Adam-mini optimizes further via Transformer-specific Hessian-based storage strategies (Zhang et al., 2024b). GaLore enhances both memory and computational efficiency through gradient matrix optimization using low-rank projections (Zhao et al., 2024), complemented by LDAdam's low-dimensional subspace optimization approach (Robert et al., 2024). Q-Galore combines quantization with low-rank projections to enhance memory and computational efficiency in resource-limited environments (Zhang et al., 2024c).

Layer-wise fine-tuning strategies have demonstrated significant effectiveness in reducing computational demands. Building upon early unsupervised approaches (Schölkopf et al., 2007; Hinton et al., 2006), LOMO introduced efficient gradient calculation and group updating (Lv et al., 2023b), while AdaLOMO enhanced this framework with adaptive learning rates (Lv et al., 2023a). LISA introduces an innovative layer importance selection strategy based on parameter norms, which further optimizes the update process (Pan et al., 2024). BAdam implemented a block coordinate optimization framework, which reduces memory consumption and computational load while improving computational efficiency by performing Adam optimization on selected parameter blocks (Luo et al., 2024). These developments highlight two crucial insights: the effectiveness of low-rank structures for sparse updates and the viability of selective layer-wise updating for efficient LLM fine-tuning.

2.2. Evolution of Adaptive Optimization Methods

First-order optimization methods play a critical role in deep learning. As one of the early foundational works, Momentum speeds up the optimization process by accumulating historical gradients (Nesterov, 1983), where RMSprop introduced the idea of adaptive learning rates, allocating distinct update steps for different parameters (Hinton et al., 2012). Adam merges the benefits of Momentum and RMSprop, adaptively adjusting both first and second moments, achieving superior convergence through adaptive moment estimation (Kingma & Ba, 2014). Building upon Adam, researchers have proposed several enhanced variants. AMSGrad (Reddi et al., 2018) strengthens optimization stability by utilizing the maximum of historical second-order moments, while NAdam (Dozat, 2016) incorporates Nesterov momentum to enhance performance. To address challenges with weight decay and learning rate adjustment in Adam, AdamW (Loshchilov, 2017) enhances L2 regularization through decoupled weight decay, and AdaBound (Luo et al., 2019) introduces learning rate bounds to prevent excessively large or small update steps. RAdam (Liu et al., 2019a) enhances convergence stability by rectifying variance estimation during the early stages of training. AdaBelief (Zhuang et al., 2020) refines the computation of second-order moments by employing the exponential moving average of gradient deviations from their mean, leading to improved generalization performance.

Recent advances have further expanded the capabilities of adaptive optimization methods. Xie et al. (2020) presents

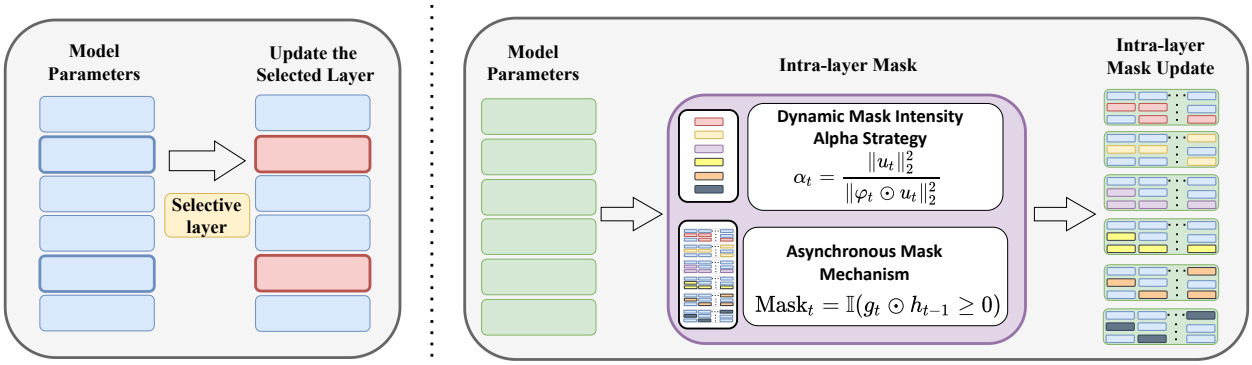

(a) Layer-wise finetuing (b) Intra-layer finetuing

Figure 1. (a) illustrates layer-wise update, where selective updates are applied to different layers. (b) shows the proposed AlphaAdam with an intra-layer update, which uses the asynchronous direction between gradients and historical momentum to determine the mask, and dynamic compensation enhances mask strength for efficient and stable updates.

the Adai framework from the perspective of dynamical systems, accelerating training and improving minima selection by decoupling the effects of adaptive learning rates and momentum. Adan (Xie et al., 2024) introduces a novel Nesterov momentum estimation method that accelerates convergence without incurring additional gradient computation overhead. Most recently, CAdam (Liang et al., 2024) proposes a synchronous masking strategy to enhance optimization efficiency, which we further extend into an asynchronous masking strategy.

2.3. Optimization Characteristics in Transformer Architecture

The Transformer architecture (Vaswani et al., 2017), which serves as the foundation for modern large-scale pre-trained models, has sparked extensive research into its structural properties and optimization dynamics. A key focus of this research has been understanding the performance differences between SGD and Adam optimization algorithms in Transformer-based models. Early investigations primarily focused on the heavy-tailed random noise encountered by SGD in language tasks (Zhang et al., 2019). However, subsequent studies revealed that a performance gap between Adam and SGD persists even when randomness is eliminated through full-batch training, potentially attributed to the sign descent mechanism (Kunstner et al., 2023). In visual tasks, particularly on the ImageNet dataset, researchers have observed that SGD consistently underperforms compared to Adam (Xiao et al., 2021), which has motivated deeper investigations into the relationships between data patterns and model architectures. Recent findings suggest that heavy-tailed class imbalance plays a crucial role in explaining Adam's superior performance over SGD in language tasks (Kunstner et al., 2024). Furthermore, researchers have discovered significant Hessian spectral differences across different parameter blocks in the Transformer model, suggesting that the Transformer's Hessian structure may exhibit block-diagonal characteristics (Zhang et al., 2024a). This observation provides a novel perspective for understanding the effectiveness of the Adam optimization algorithm in Transformer architectures.

3. Methodology

3.1. Preliminaries

3.1.1. Theoretical Basis

As discussed in the introduction, asynchronous behavior between gradients and momentum plays a crucial role in practical optimization. To rigorously analyze this phenomenon and establish our theoretical framework, we first need to characterize how parameter updates affect the loss landscape. Consider the second-order Taylor expansion of the loss function $\mathcal{L}(\theta)$ at the parameter θ_t in Transformer optimization. Let $\Delta\theta = \theta_t - \theta_{t+1}$ denote the parameter update. The local quadratic approximation is given by:

$$\mathcal{L}(\theta_{t+1}) \approx \mathcal{L}(\theta_t) + \nabla\mathcal{L}(\theta_t)^\top \Delta\theta + \frac{1}{2}\Delta\theta^\top \nabla^2\mathcal{L}(\theta_t)\Delta\theta \quad (1)$$

where $\mathcal{L}(\theta_t)$ is the current loss value, $\nabla\mathcal{L}(\theta_t)^\top\Delta\theta$ represents the first-order term, and $\frac{1}{2}\Delta\theta^\top\nabla^2\mathcal{L}(\theta_t)\Delta\theta$ captures the second-order curvature information through the Hessian matrix.

Following (Pan, 2023), we formally define two key metrics to characterize the properties of parameter updates:

Definition 3.1. (*Gradient Correlation* (**GC**)). For a parameter update $\Delta\theta$, the GC at point θ_t in the parameter space is

defined as:

$$\mathrm{GC}(\theta_t, \Delta\theta) = \Delta\theta^\top \nabla \mathcal{L}(\theta_t) \tag{2}$$

Definition 3.2. (*Directional Sharpness* (**DS**)). For a parameter update direction $\Delta\theta$, the DS at point θ_t in the parameter space is defined as:

$$\mathrm{DS}(\theta_t, \Delta\theta) = \Delta\theta^\top \nabla^2 \mathcal{L}(\theta_t) \Delta\theta \tag{3}$$

As suggested by Pan (2023), lower DS and higher GC are beneficial for loss decrease, which aligns with our theoretical findings about the effectiveness of asynchronous masking strategies.

3.1.2. Hessian Properties of Transformers

For the Transformer architecture,Theorem Zhang et al. (2024a) argue that the Transformer can be upper approximated by a block-diagonal structure. Based on this property, we observe the following properties of its optimization landscape:

Theorem 3.3. *(Transformer Directional Sharpness). For the Transformer architecture, there exist constants $c_1, c_2 > 0$ such that the directional sharpness is bounded by:*

$$c_1 \|\Delta\theta\|^2 \leq ds(\theta_t, \Delta\theta) \leq c_2 \|\Delta\theta\|^2 \tag{4}$$

This crucial property indicates that in Transformer optimization, the directional sharpness is proportional to the square of the parameter update magnitude. Detailed proofs are provided in the appendix A.

Corollary 3.4. *Under the conditions specified in Theorem 3.3, momentum masking demonstrates enhanced stability compared to momentum gradients, with the following quantitative characteristics:*

- *The variance of parameter updates is reduced by a factor of $\frac{(1-\beta)^2}{1-\beta^2} < 1$, indicating a decrease in variance*
- *The off-diagonal terms in the update matrix are suppressed by a factor of $\left(\frac{(1-\beta)^2}{1-\beta^2}\right)^2$, further decreasing instability during the update*

where $\beta \in (0, 1)$ is the momentum coefficient 0.9 to 0.99 in practice.

Detailed proofs are provided in the appendix B.

3.2. Dynamic Alpha Asynchronous Masking Mechanism

3.2.1. Asynchronous Masking Strategy

To address the optimization challenges in large-scale neural networks, we propose a novel asynchronous masking mechanism, which aims to better utilize historical information and improve the stability of parameter updates. Parameter masking strategies play a crucial role in optimization by determining which parameters to update in each iteration. We compare two approaches: the traditional synchronous masking and our proposed asynchronous masking strategy.

Specifically, the traditional synchronous masking strategy (**Setting 1**) decides the mask based on the current momentum and gradient:

$$\phi_i = \begin{cases} 1 & \text{if } m_t^{(i)} g_t^{(i)} \geq 0 \\ 0 & \text{otherwise} \end{cases} \tag{5}$$

where $m_t^{(i)}$ and $g_t^{(i)}$ denote the momentum and gradient components at time t, respectively.

In contrast, the asynchronous masking strategy (**Setting 2**) we propose uses momentum from past time steps to determine the mask:

$$\phi_i = \begin{cases} 1 & \text{if } m_{t-1}^{(i)} g_t^{(i)} \geq 0 \\ 0 & \text{otherwise} \end{cases} \tag{6}$$

To analyze these strategies, we define the following sets:

- S_1: The set of elements with mask 1 in Setting 1, indicating that the momentum and gradient have the same sign at the current time step;
- S_2: The set of elements with mask 1 in Setting 2, representing elements where the momentum and gradient have the same sign at historical time steps;
- S_{12}: The set of elements with mask 1 in both settings;
- S_{11}: The set of elements with mask 1 only in Setting 1 ($S_1 \setminus S_{12}$)

Based on above sets, the following theorem can be derived:

Theorem 3.5. *(Optimality of Asynchronous Masking) Let $E[g_i^2] = \sigma_i^2$ be the second-order moment of gradients and $E[g_i m_{t-1,i}] = \rho_i \sigma_i^2$ be the correlation between gradients and historical momentum, where ρ_i denotes the correlation coefficient. Under momentum updates $m_t = \beta_1 m_{t-1} + (1-\beta_1) g_t$, the asynchronous masking strategy outperforms the synchronous masking strategy.*

Detailed proofs are provided in the appendix C. Under these conditions, the asynchronous masking strategy strengthens the correlation of gradients, enhances optimization performance, and improves system stability by reducing the directional sharpness of the updates.

3.2.2. DYNAMIC ALPHA STRATEGY

To bridge the gap between theoretical analysis and practical implementation of asynchronous or synchronous masking strategy of parameter updates, we introduce a dynamic compensation mechanism. Our key observation is that mask-based updates, while theoretically sound in continuous-time frameworks, lead to reduced update magnitudes in discrete implementations, potentially slowing down convergence and weakening the theoretical guarantees.

First, Consider the continuous-time dynamics described by the Lyapunov stability theorem:

$$\frac{\mathrm{d}}{\mathrm{d}t}\mathcal{H} = -\Delta_{\mathcal{H}} \tag{7}$$

where $\mathcal{H}$ denotes the Lyapunov function characterizing the system's stability, and $\Delta_{\mathcal{H}}$ represents the instantaneous rate of change. When implementing mask-based updates in discrete time steps, the effective update magnitude is inherently reduced due to the masking operation, causing a discrepancy from the theoretical continuous-time framework.

To compensate for this reduction in update magnitude, we propose a dynamically adjusted system:

$$\frac{\mathrm{d}}{\mathrm{d}t}\mathcal{H}_c = -\alpha(t)\Delta\mathcal{H} \tag{8}$$

where $\mathcal{H}_c$ represents the compensated system state. The compensation factor $\alpha(t)$ is specifically designed to counterbalance the magnitude reduction caused by masking:

$$\alpha(t) = \sqrt{\frac{\sum_{i=1}^{d} u_i^2}{\sum_{i\in S} u_i^2}} \tag{9}$$

where u_i denotes the i-th component of the parameter update, and S represents the subset of parameters selected by the masking strategy. This design directly compensates for the magnitude reduction by scaling the updates according to the ratio between the full update norm and the masked update norm.

Theorem 3.6. *(Properties of Adaptive Compensation) Under the conditions of Theorem 3.3 and for sufficiently large dimension d, the following properties hold:*

- *The compensation factor exhibits controlled scaling behavior with respect to the learning rate η:*

$$\frac{\partial\alpha(t)}{\partial\eta} = \mathcal{O}(\|D\|_2) + \mathcal{O}(\varepsilon)$$
$$\frac{\partial^2\alpha(t)}{\partial\eta^2} = \mathcal{O}(\|D\|_2^2) + \mathcal{O}(\varepsilon\|D\|_2^2)$$

  where D represents the diagonal component of the Hessian matrix

- *In the high-dimensional limit, the gradient directions of η and α are approximately orthogonal: For any $\varepsilon > 0$, with probability at least $1-\delta$,*

$$\frac{v_\eta^T v_\alpha}{\|v_\eta\|\|v_\alpha\|} \le \varepsilon$$

  where v_η and v_α denote the gradient vectors with respect to η and α respectively

This theorem explains two key motivations behind the use of $\alpha(t)$:

Magnitude Restoration: The first property shows that $\alpha(t)$ scales appropriately with the learning rate, ensuring that the compensation remains effective across different optimization settings. The dependence on the Hessian diagonal D indicates that the compensation adapts to local geometric properties of the loss landscape.

Trajectory Preservation: The second property, establishing approximate orthogonality between gradients of η and α, ensures that our compensation mechanism does not interfere with the original optimization trajectory. This preservation is crucial for maintaining the theoretical guarantees derived from the continuous-time framework.

In essence, our compensation mechanism provides a principled approach to maintain the theoretical benefits of mask-based updates while addressing the practical challenges of discrete implementation. Detailed proofs are provided in Appendix D.

3.2.3. ALGORITHM DESCRIPTION

Based on the Optimality of Asynchronous Masking (3.5) and the Properties of Adaptive Compensation Theorem (3.6) , we propose the AlphaAdam algorithm, with its pseudocode as shown in Algorithm 1.

The two main innovations of the algorithm are:

- The asynchronous masking strategy, which uses actual historical gradient information to improve the timing of parameter updates, thus enhancing the masking effect and ensuring that the optimization process is superior to the traditional synchronous masking strategy.

- The introduction of the dynamic compensation factor $\alpha(t)$, which effectively regulates the geometric properties of parameter updates and ensures the stability and convergence of the optimization process through its combination with the high-dimensional orthogonality of the learning rate.

Algorithm 1 Alpha Adam Method

Input: Learning rate $\eta > 0$, initial parameters θ_0, loss function $\mathcal{L}(\theta)$, momentum factors $\beta_1, \beta_2 \in [0, 1)$, stability term $\epsilon > 0$,parameter dimension d.
for $t = 1$ **to** T **do**
  $g_t = \nabla\mathcal{L}(\theta_t)$
  $d_t = g_t \odot h_{t-1}$
  $h_t = \beta_1 h_{t-1} + (1 - \beta_1)g_t$
  $v_t = \beta_2 v_{t-1} + (1 - \beta_2)(g_t \odot g_t)$
  $u_t = \frac{h_t}{\sqrt{v_t}+\epsilon}$
  $\varphi_t = \mathbb{I}(d_t > 0)$
  $\alpha_t = \frac{\|u_t\|_2^2}{\|\varphi_t \odot u_t\|_2^2}$
  $\hat{\eta} = \eta \frac{d}{\|\varphi\|_0+1}$
  $\theta_{t+1} = \theta_t - \hat{\eta}\alpha_t\varphi_t \odot u_t$
end for
Return: Final parameters θ_T

3.2.4. Convergence guarantee

In this section, we present the convergence analysis for AlphaAdam under standard optimization assumptions in the context of full-batch training. Our analysis relies on the fundamental smoothness property of the objective function:

Assumption 3.7. The objective function $\mathcal{L}$ is L-smooth and non-negative, i.e., for any $x, y \in \mathbb{R}^d$:

$$\|\nabla\mathcal{L}(x) - \nabla\mathcal{L}(y)\| \leq L\|x - y\|$$

Under L-smoothness assumption, we establish the main convergence guarantee for AlphaAdam:

Theorem 3.8. *For the full-batch AlphaAdam algorithm, assuming that Assumptions3.7 hold, and* $\beta_1 < \sqrt{\beta_2} < 1$ *with the step size* $\eta_t = \frac{\eta}{\sqrt{t}}$*, the following holds:*

$$\min_{t\in(1,T]} \|\nabla\mathcal{L}_t\|_\varphi \leq \mathcal{O}\left(\frac{\log T}{\sqrt{T}}\right)$$

Detailed proofs are provided in the appendix E. It demonstrates that AlphaAdam achieves a convergence rate of $\mathcal{O}(\frac{\log T}{\sqrt{T}})$, matching the order-wise convergence rate of standard Adam in non-convex settings. The norm $\|\cdot\|_\varphi$ measures the gradient magnitude over dimensions selected by the adaptive mask, providing a natural metric for tracking convergence under our masking mechanism. Specifically, $\|\nabla\mathcal{L}_t\|_\varphi$ represents the effective gradient norm after masking, reflecting the optimization progress in active dimensions where the mask values are 1.

The condition $\beta_1 < \sqrt{\beta_2}$ serves as a necessary requirement for convergence(Zhang et al., 2022; Wang et al., 2023), consistent with previous analyses of Adam-type algorithms. We employ the standard decaying step size schedule $\eta_t = \frac{\eta}{\sqrt{t}}$ to ensure proper balance between exploration and exploitation during training.

The norm of the effective gradient converges to zero at the rate of $\mathcal{O}(\frac{\log T}{\sqrt{T}})$. The theoretical relationship between the overall gradient norm and the effective gradient norm also requires careful handling in the theoretical analysis.

Notably, our convergence guarantee holds without requiring additional assumptions on the masking mechanism, suggesting that our adaptive masking strategy preserves essential convergence properties while offering potential computational benefits. It is worth noting that our current analysis focuses on the full-batch setting. Extending these results to the stochastic gradient case would require additional consideration of gradient variance effects. Furthermore, quantifying the impact of masking ratios on convergence rates remains an interesting direction for future theoretical investigation.

4. Experiments

4.1. Experimental Setup

The Experiments section focuses on evaluating the performance of Alpha Adam, particularly on key tasks related to large language models, including pretraining and supervised fine-tuning (SFT). All experiments were conducted on two NVIDIA V100-32GB GPUs, with detailed experimental setups provided in the appendix.

To comprehensively evaluate the performance of AlphaAdam, we compared it with several optimizers, including AdamW(Loshchilov, 2017), CAdam(Liang et al., 2024),as well as other state-of-the-art memory-efficient optimization methods such as GaLore(Zhao et al., 2024), LDAdam(Robert et al., 2024) and Adam mini(Zhang et al., 2024b).

During the experiment, all comparative tests maintained the same configuration and settings. Under the same computational budget, we adjusted the learning rate of all methods and reported their best performance.

4.2. Pretraining Performance of GPT-2

During the pretraining experiments, we utilized the open-source GPT-2 series models and trained them from scratch on mainstream English corpora. Specifically, the GPT-2 series models(Radford et al., 2019) were pretrained on the OpenWebText dataset(Gokaslan et al., 2019) to ensure the reproducibility and consistency of the results. To evaluate the performance, we conducted pretraining experiments on GPT-2 models of different scales (125M, 355M, 744M parameters). As shown in Figure 2, the training curves demonstrate that AlphaAdam consistently achieved the optimal loss reduction across all model scales, outperforming other optimization methods in terms of convergence speed

Table 1. Comparison of results of fine-tuning RoBERTa-base model on GLUE benchmark

Method	MRPC	STS-B	CoLA	RTE	SST-2	QNLI	QQP	Avg.
AdamW	**89.17**	89.65	**58.04**	68.23	94.24	92.4	90.97	83.24
Adam-mini	87.01	88.15	55.30	56.32	93.35	92.02	89.79	80.28
GaLore (rank=8)	86.19	88.97	55.12	69.45	94.15	92.01	89.86	82.25
LDAdam (rank=8)	88.32	90.03	60.60	67.58	**94.49**	**92.82**	91.23	83.58
CAdamW	88.48	89.65	54.60	70.12	90.98	92.04	91.13	82.42
AlphaAdam	88.97	**90.42**	57.25	**71.49**	93.35	92.18	**91.76**	**83.63**

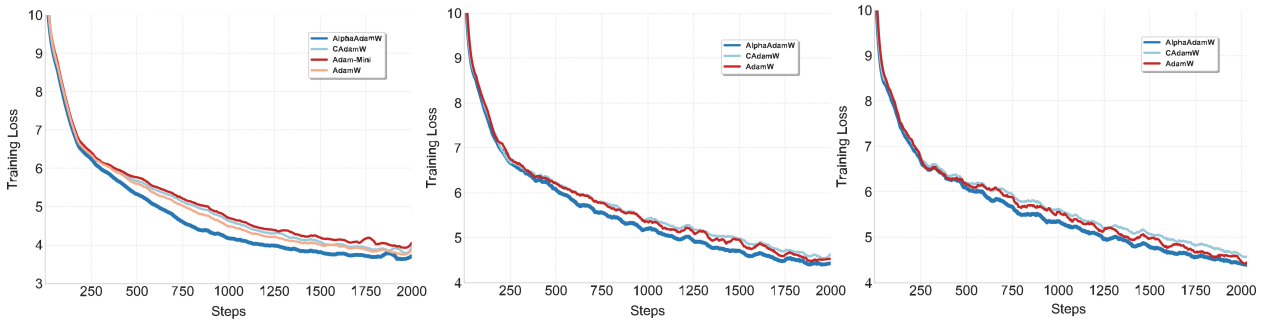

GPT2 125M Training Loss GPT2 355M Training Loss GPT2 744M Training Loss

Figure 2. GPT-2 model pre-trained on the OpenWebText dataset. Loss curves for different sizes of training steps are reported.

Table 2. Fine-tuning results for Llama-2 on GSM-8k.

Model	Metric	Adam	Adam-8b	LDAdam ($rank = 512$)	GALore ($rank = 512$)	CAdam	MicroAdam ($m = 10$)	AlphaAdam
7B	Accuracy	34.53	34.42	34.88	34.62	34.68	34.58	**34.94**
	Train loss	0.064	0.069	0.073	0.070	0.081	0.057	**0.048**

and final loss values.

4.3. Moderate Scale Fine-tuning

To further validate the effectiveness of AlphaAdam, we conducted comprehensive experiments on downstream tasks, with particular emphasis on supervised fine-tuning (SFT) scenarios. Our evaluation encompassed two representative tasks: fine-tuning the RoBERTa-base model(Liu et al., 2019b) on the GLUE benchmark and the Llama2-7b model(Touvron et al., 2023) on the GSM8K.

4.3.1. GLUE Benchmark

The GLUE benchmark, comprising diverse NLU tasks with varying dataset sizes and complexity levels, serves as a comprehensive metric for evaluating model performance and generalization capabilities across different linguistic challenges.

Through systematic learning rate tuning between 1e-5 and 5e-5, AlphaAdam achieved state-of-the-art performance with an average GLUE score of 83.63, surpassing the baseline AdamW score of 83.24.

AlphaAdam demonstrated consistent improvements across datasets of varying scales. On the small-scale RTE dataset, AlphaAdam achieved an accuracy of 71.49% compared to AdamW's 68.23%. Similarly, for the large-scale QQP dataset, AlphaAdam reached 91.76% accuracy versus AdamW's 90.97%. The model maintained remarkably stable performance with task variance below 0.05%, highlighting its robust generalization capabilities across diverse NLP applications.

4.3.2. Llama-2 Fine-tuning on GSM8K Dataset

We evaluate AlphaAdam on fine-tuning Llama2-7B model on GSM-8K. The Llama2 model is a decoder-only large language model based on the attention mechanism, widely used for fine-tuning various NLP tasks (Touvron et al., 2023).GSM-8K is a challenging grade-school-level math-

ematical reasoning dataset, and given the extremely low zero-shot accuracy of the base models on this task, the post-fine-tuning performance serves as a crucial indicator for assessing fine-tuning strategies(Cobbe et al., 2021).We perform learning rate grid search across 1e-5 to 5e-4,the same as in (Robert et al., 2024).

As shown in Table 2, AlphaAdam achieves state-of-the-art accuracy of 34.94% on the 7B-parameter model, surpassing existing optimization approaches. Notably, AlphaAdam also achieves the lowest training loss of 0.048, demonstrating its superior optimization capabilities.

Figure 3 illustrates AlphaAdam's exceptional optimization dynamics, showing marked performance gains after the second epoch and exhibiting notably faster convergence, which validates AlphaAdam's effectiveness in navigating the complex optimization landscape of large language models while maintaining computational efficiency.

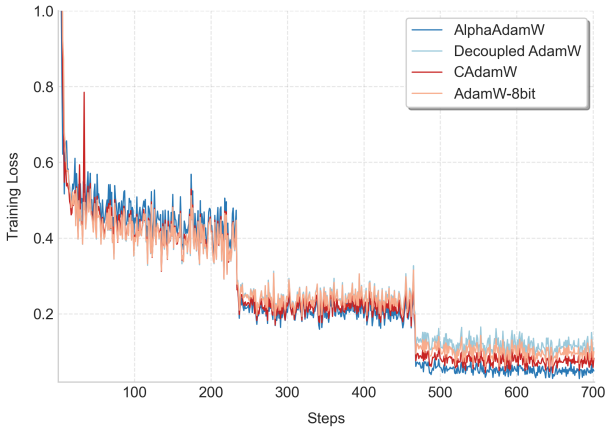

Figure 3. Llama2-7B GSM8K Fine-tuning Loss Curves.

4.4. Ablation Study

To validate the effectiveness of the components we propose, we conduct a comprehensive ablation study on GPT2-125M pretraining over 10k steps. Table 3 presents the average validation loss across different configurations, comparing our method with several variants. We observe that the synchronized masking variant with Adam optimization exhibits marginally elevated validation loss (Early: 3.646, Late: 3.269) compared to the baseline Adam configuration (Early: 3.610, Late: 3.243). This performance gap is substantially bridged through asynchronous masking, which reduces early-phase validation loss by 1.5% to 3.554 while maintaining late-phase parity with standard Adam. The complete methodological framework—integrating asynchronous masking with dynamic α-strength adaptation—achieves optimal performance (Early: 3.523, Late: 3.237), establishing a 2.4% improvement over baseline during critical early optimization stages. Basically the ablation study results empirically validate our theoretical analysis about the benefits of asynchronous masking and dynamic strength adjustment.The performance gain from asynchronous masking aligns with our GC and DS analysis, and the further improvement from dynamic α highlights the importance of adaptively balancing these factors during training.

Table 3. Comparison of Validation Loss at Different Steps for Different Methods, where *SM* denotes Synchronized Mask mechanismand *AM* denotes Asynchronous Mask mechanism.

Methods	**Step**	**Val Loss**	**Step**	**Val Loss**
Baseline	20%	3.799	60%	3.288
AdamW	40%	3.420	100%	3.198
	Avg(Early)	3.610	Avg(Late)	3.243
AdamW	20%	3.850	60%	3.310
+*SM*	40%	3.442	100%	3.227
	Avg(Early)	3.646	Avg(Late)	3.269
Our AdamW	20%	3.717	60%	3.282
+*AM*	40%	3.391	100%	3.213
	Avg(Early)	3.554	Avg(Late)	3.247
Our AdamW	20%	3.658	60%	3.271
+*AM*	40%	3.374	100%	3.203
+*Dynamic* α	Avg(Early)	**3.523**	Avg(Late)	**3.237**

5. Conclusion

In this study, we proposed asynchronous masking and dynamic masking strength strategies, and introduced an Adam variant, AlphaAdam, based on these strategies. We thoroughly analyzed the convergence properties of these methods and validated the effectiveness of the algorithm through a series of LLM experiments. The experimental results show that AlphaAdam exhibits faster convergence and more stable loss reduction during training, offering significant advantages compared to existing Adam-based algorithms.

Our approach is particularly suitable for tasks that require accelerated convergence or improved stability, especially in LLM training. By combining asynchronous masking and dynamic masking strength strategies, AlphaAdam significantly enhances performance across multiple optimization processes, reduces training time, and demonstrates better generalization capabilities on various datasets.

Moreover, while this study mainly focuses on validating the convergence and effectiveness of AlphaAdam, our strategies also have broad potential applications.

6. Impact Statement

This work advances Machine Learning by proposing AlphaAdam, an efficient optimization algorithm for large-scale language models, reducing computational costs and improving training stability. These advancements contribute to more sustainable and accessible AI development.

References

Cobbe, K., Kosaraju, V., Bavarian, M., Chen, M., Jun, H., Kaiser, L., Plappert, M., Tworek, J., Hilton, J., Nakano, R., et al. Training verifiers to solve math word problems. *arXiv preprint arXiv:2110.14168*, 2021.

Dozat, T. Incorporating nesterov momentum into adam. 2016.

Gokaslan, A., Cohen, V., Pavlick, E., and Tellex, S. Openwebtext corpus. http://Skylion007.github.io/OpenWebTextCorpus, 2019.

Gur-Ari, G., Roberts, D. A., and Dyer, E. Gradient descent happens in a tiny subspace. *arXiv preprint arXiv:1812.04754*, 2018.

Hinton, G., Srivastava, N., and Swersky, K. Lecture 6a overview of mini–batch gradient descent. *Coursera Lecture slides https://class. coursera. org/neuralnets-2012-001/lecture,[Online*, 2012.

Hinton, G. E., Osindero, S., and Teh, Y.-W. A fast learning algorithm for deep belief nets. *Neural Computation*, 18 (7):1527–1554, 2006. doi: 10.1162/neco.2006.18.7.1527.

Kingma, D. P. and Ba, J. Adam: A method for stochastic optimization. *CoRR*, abs/1412.6980, 2014. URL https://api.semanticscholar.org/CorpusID:6628106.

Kunstner, F., Chen, J., Lavington, J. W., and Schmidt, M. W. Noise is not the main factor behind the gap between sgd and adam on transformers, but sign descent might be. *ArXiv*, abs/2304.13960, 2023. URL https://api.semanticscholar.org/CorpusID:258352540.

Kunstner, F., Yadav, R., Milligan, A., Schmidt, M., and Bietti, A. Heavy-tailed class imbalance and why adam outperforms gradient descent on language models. *ArXiv*, abs/2402.19449, 2024. URL https://api.semanticscholar.org/CorpusID:268091204.

Larsen, B. W., Fort, S., Becker, N., and Ganguli, S. How many degrees of freedom do we need to train deep networks: a loss landscape perspective. *ArXiv*, abs/2107.05802, 2021.

Liang, K., Chen, L., Liu, B., and Liu, Q. Cautious optimizers: Improving training with one line of code. *ArXiv*, abs/2411.16085, 2024. URL https://api.semanticscholar.org/CorpusID:274234738.

Liu, L., Jiang, H., He, P., Chen, W., Liu, X., Gao, J., and Han, J. On the variance of the adaptive learning rate and beyond. *ArXiv*, abs/1908.03265, 2019a. URL https://api.semanticscholar.org/CorpusID:199528271.

Liu, Y., Ott, M., Goyal, N., Du, J., Joshi, M., Chen, D., Levy, O., Lewis, M., Zettlemoyer, L., and Stoyanov, V. Roberta: A robustly optimized bert pretraining approach. *ArXiv*, abs/1907.11692, 2019b. URL https://api.semanticscholar.org/CorpusID:198953378.

Liu, Y., Agarwal, S., and Venkataraman, S. Autofreeze: Automatically freezing model blocks to accelerate fine-tuning. *ArXiv*, abs/2102.01386, 2021.

Loshchilov, I. Decoupled weight decay regularization. *arXiv preprint arXiv:1711.05101*, 2017.

Luo, L., Xiong, Y., Liu, Y., and Sun, X. Adaptive gradient methods with dynamic bound of learning rate. *ArXiv*, abs/1902.09843, 2019. URL https://api.semanticscholar.org/CorpusID:67856101.

Luo, Q., Yu, H., and Li, X. Badam: A memory efficient full parameter optimization method for large language models. In *The Thirty-eighth Annual Conference on Neural Information Processing Systems*, 2024.

Lv, K., Yan, H., Guo, Q., Lv, H., and Qiu, X. Adalomo: Low-memory optimization with adaptive learning rate. *ArXiv*, abs/2310.10195, 2023a. URL https://api.semanticscholar.org/CorpusID:264147071.

Lv, K., Yang, Y., Liu, T., Gao, Q., Guo, Q., and Qiu, X. Full parameter fine-tuning for large language models with limited resources. In *Annual Meeting of the Association for Computational Linguistics*, 2023b.

Nesterov, Y. A method for solving the convex programming problem with convergence rate $o(1/k^2)$. *Proceedings of the USSR Academy of Sciences*, 269:543–547, 1983. URL https://api.semanticscholar.org/CorpusID:145918791.

Pan, R., Liu, X., Diao, S., Pi, R., Zhang, J., Han, C., and Zhang, T. Lisa: Layerwise importance sampling for memory-efficient large language model fine-tuning. *arXiv preprint arXiv:2403.17919*, 2024.

Pan, Y. Toward understanding why adam converges faster than sgd for transformers. *ArXiv*, abs/2306.00204, 2023. URL https://api.semanticscholar.org/CorpusID:254223828.

Radford, A., Wu, J., Child, R., Luan, D., Amodei, D., and Sutskever, I. Language models are unsupervised multitask learners. 2019. URL https://api.semanticscholar.org/CorpusID:160025533.

Reddi, S. J., Kale, S., and Kumar, S. On the convergence of adam and beyond. *ArXiv*, abs/1904.09237, 2018. URL https://api.semanticscholar.org/CorpusID:3455897.

Robert, T., Safaryan, M., Modoranu, I.-V., and Alistarh, D. Ldadam: Adaptive optimization from low-dimensional gradient statistics. *ArXiv*, abs/2410.16103, 2024.

Schölkopf, B., Platt, J., and Hofmann, T. *Greedy Layer-Wise Training of Deep Networks*, pp. 153–160. 2007.

Shazeer, N. and Stern, M. Adafactor: Adaptive learning rates with sublinear memory cost. In *International Conference on Machine Learning*, pp. 4596–4604. PMLR, 2018.

Shi, N., Li, D., Hong, M., and Sun, R. Rmsprop converges with proper hyper-parameter. In *International Conference on Learning Representations*, 2021. URL https://api.semanticscholar.org/CorpusID:235420301.

Touvron, H., Martin, L., Stone, K., Albert, P., Almahairi, A., Babaei, Y., Bashlykov, N., Batra, S., Bhargava, P., Bhosale, S., et al. Llama 2: Open foundation and fine-tuned chat models. *arXiv preprint arXiv:2307.09288*, 2023.

Vaswani, A., Shazeer, N. M., Parmar, N., Uszkoreit, J., Jones, L., Gomez, A. N., Kaiser, L., and Polosukhin, I. Attention is all you need. In *Neural Information Processing Systems*, 2017. URL https://api.semanticscholar.org/CorpusID:13756489.

Wang, B., Fu, J., Zhang, H., Zheng, N., and Chen, W. Closing the gap between the upper bound and the lower bound of adam's iteration complexity. *ArXiv*, abs/2310.17998, 2023. URL https://api.semanticscholar.org/CorpusID:264555523.

Xiao, T., Singh, M., Mintun, E., Darrell, T., Dollár, P., and Girshick, R. B. Early convolutions help transformers see better. In *Neural Information Processing Systems*, 2021. URL https://api.semanticscholar.org/CorpusID:235658393.

Xie, X., Zhou, P., Li, H., Lin, Z., and Yan, S. Adan: Adaptive nesterov momentum algorithm for faster optimizing deep models. *IEEE Transactions on Pattern Analysis and Machine Intelligence*, 46(12):9508–9520, 2024. doi: 10.1109/TPAMI.2024.3423382.

Xie, Z., Wang, X., Zhang, H., Sato, I., and Sugiyama, M. Adaptive inertia: Disentangling the effects of adaptive learning rate and momentum. In *International Conference on Machine Learning*, 2020. URL https://api.semanticscholar.org/CorpusID:248986834.

Zhang, J., Karimireddy, S. P., Veit, A., Kim, S., Reddi, S. J., Kumar, S., and Sra, S. Why adam beats sgd for attention models. *ArXiv*, abs/1912.03194, 2019. URL https://api.semanticscholar.org/CorpusID:208858389.

Zhang, Y., Chen, C., Shi, N., Sun, R., and Luo, Z. Adam can converge without any modification on update rules. *ArXiv*, abs/2208.09632, 2022. URL https://api.semanticscholar.org/CorpusID:251718882.

Zhang, Y., Chen, C., Ding, T., Li, Z., Sun, R., and Luo, Z. Why transformers need adam: A hessian perspective. *ArXiv*, abs/2402.16788, 2024a. URL https://api.semanticscholar.org/CorpusID:268032936.

Zhang, Y., Chen, C., Li, Z., Ding, T., Wu, C., Ye, Y., Luo, Z.-Q., and Sun, R. Adam-mini: Use fewer learning rates to gain more. *arXiv preprint arXiv:2406.16793*, 2024b.

Zhang, Z. A., Jaiswal, A. K., Yin, L., Liu, S., Zhao, J., Tian, Y., and Wang, Z. Q-galore: Quantized galore with int4 projection and layer-adaptive low-rank gradients. *ArXiv*, abs/2407.08296, 2024c. URL https://api.semanticscholar.org/CorpusID:271097500.

Zhao, J., Zhang, Z., Chen, B., Wang, Z., Anandkumar, A., and Tian, Y. Galore: Memory-efficient llm training by gradient low-rank projection. *arXiv preprint arXiv:2403.03507*, 2024.

Zhuang, J., Tang, T. M., Ding, Y., Tatikonda, S. C., Dvornek, N. C., Papademetris, X., and Duncan, J. S. Adabelief optimizer: Adapting stepsizes by the belief in observed gradients. *ArXiv*, abs/2010.07468, 2020. URL https://api.semanticscholar.org/CorpusID:222377595.

In this appendix, we provide detailed proofs of all theoretical results presented in the main paper.

- Section A proves the block-diagonal approximation properties (Theorem 3.3), which forms the foundation for our geometric analysis.
- Section B analyzes the momentum method under block structure (Corollary 3.4), demonstrating how momentum affects parameter updates in different subspaces.
- Section C provides theoretical comparisons of different masking strategies (Theorem 3.5), with particular attention to their application in LLM training.
- Section D presents the analysis of dynamic compensation factors (Theorem 3.6), showing why both learning rate and dynamic compensation are necessary.
- Section E presents the convergence analysis (Theorem 3.8) of our proposed algorithm, establishing its theoretical guarantees.
- Section F provides more experimental details of LLM fine-tuning and pre-training.

A. Block-Diagonal Approximation Properties

A.1. Assumptions: Block-Diagonal Approximability

Assumption A.1. We assume that for the Transformer model, the Hessian matrix $H = \nabla^2 \mathcal{L}(\theta_t)$ can be approximated by a block diagonal matrix with an additional non-diagonal perturbation term. Specifically, there exists a block partitioning of the parameters such that:

$$H = D + E$$

where D is a block diagonal matrix, and E is a non-diagonal perturbation matrix. Furthermore, we assume the perturbation matrix E satisfies the following bound:

$$\|E\|_2 \leq \varepsilon \|D\|_2$$

for some constant $\varepsilon \in (0, 1)$.

Assumption A.2. We assume that the eigenvalues of each diagonal block H_{ii} of D are bounded. Specifically, for each i, there exist constants $\mu_i > 0$ and $\sigma_i \in (0, 1)$ such that all eigenvalues λ_{ij} of H_{ii} satisfy:

$$(1 - \sigma_i)\mu_i \leq \lambda_{ij} \leq (1 + \sigma_i)\mu_i$$

Additionally, we assume the following boundary conditions for the parameters:

- $c_{\min} \leq \mu_i \leq c_{\max}$, for all blocks i, where $0 < c_{\min} \leq c_{\max}$
- $\sigma_i \leq \sigma_{\max} < 1$, for all i
- $\|\Delta\theta_i\|_2 \leq M$, for some constant M, for all parameter blocks i

A.2. Proof of Theorem 3.3

Theorem A.3. *(Directional Sharpness of the Transformer). For the Transformer architecture, there exist constants $c_1, c_2 > 0$ such that the directional sharpness is bounded as:*

$$c_1 \|\Delta\theta\|^2 \leq ds(\theta_t, \Delta\theta) \leq c_2 \|\Delta\theta\|^2$$

where $ds(\theta_t, \Delta\theta)$ represents the sharpness of the direction, and $\|\Delta\theta\|^2$ denotes the squared norm of the parameter update $\Delta\theta$.

To ensure that $\alpha > 0$, the following condition on ε must hold:

$$\varepsilon < \frac{(1-\sigma_{\max})c_{\min}}{(1+\sigma_{\max})c_{\max}}$$

Proof. The quadratic form of the block diagonal matrix D is bounded as follows. For each diagonal block H_{ii}, using the eigenvalue distribution property from Assumption A.2, we get:

$$(1-\sigma_i)\mu_i\|\Delta\theta_i\|_2^2 \leq \Delta\theta_i^\top H_{ii}\Delta\theta_i \leq (1+\sigma_i)\mu_i\|\Delta\theta_i\|_2^2$$

Summing over all blocks, we obtain:

$$\sum_{i=1}^{k}(1-\sigma_i)\mu_i\|\Delta\theta_i\|_2^2 \leq \Delta\theta^\top D\Delta\theta \leq \sum_{i=1}^{k}(1+\sigma_i)\mu_i\|\Delta\theta_i\|_2^2$$

Since $\sigma_i \leq \sigma_{\max}$, $\mu_i \geq c_{\min}$, and $\mu_i \leq c_{\max}$, we have:

$$(1-\sigma_{\max})c_{\min}\sum_{i=1}^{k}\|\Delta\theta_i\|_2^2 \leq \Delta\theta^\top D\Delta\theta \leq (1+\sigma_{\max})c_{\max}\sum_{i=1}^{k}\|\Delta\theta_i\|_2^2$$

For the non-diagonal matrix E, by Assumption A.1, we use the Cauchy-Schwarz inequality to obtain:

$$|\Delta\theta^\top E\Delta\theta| \leq \|E\|_2\|\Delta\theta\|_2^2 \leq \varepsilon\|D\|_2\|\Delta\theta\|_2^2$$

Since $\|D\|_2 \leq (1+\sigma_{\max})c_{\max}$, this gives:

$$|\Delta\theta^\top E\Delta\theta| \leq \varepsilon(1+\sigma_{\max})c_{\max}\sum_{i=1}^{k}\|\Delta\theta_i\|_2^2$$

Combining the bounds for D and E, we get the overall bounds for the directional sharpness ds. Specifically:

$$ds = \Delta\theta^\top H\Delta\theta = \Delta\theta^\top D\Delta\theta + \Delta\theta^\top E\Delta\theta$$

Thus, we have:

$$\begin{aligned} ds &\geq (1-\sigma_{\max})c_{\min}\sum_{i=1}^{k}\|\Delta\theta_i\|_2^2 - \varepsilon(1+\sigma_{\max})c_{\max}\sum_{i=1}^{k}\|\Delta\theta_i\|_2^2 \\ &= [(1-\sigma_{\max})c_{\min} - \varepsilon(1+\sigma_{\max})c_{\max}]\sum_{i=1}^{k}\|\Delta\theta_i\|_2^2 \end{aligned}$$

Let $\alpha = (1-\sigma_{\max})c_{\min} - \varepsilon(1+\sigma_{\max})c_{\max}$, so that:

$$ds \geq \alpha\sum_{i=1}^{k}\|\Delta\theta_i\|_2^2$$

Similarly:

$$ds \leq (1+\sigma_{\max})c_{\max}\sum_{i=1}^{k}\|\Delta\theta_i\|_2^2 + \varepsilon(1+\sigma_{\max})c_{\max}\sum_{i=1}^{k}\|\Delta\theta_i\|_2^2$$
$$= (1+\sigma_{\max})c_{\max}(1+\varepsilon)\sum_{i=1}^{k}\|\Delta\theta_i\|_2^2$$

Let $\beta = (1+\sigma_{\max})c_{\max}(1+\varepsilon)$, so that:

$$ds \leq \beta\sum_{i=1}^{k}\|\Delta\theta_i\|_2^2$$

To ensure that $\alpha > 0$, we require the condition:

$$\varepsilon < \frac{(1-\sigma_{\max})c_{\min}}{(1+\sigma_{\max})c_{\max}}$$

This guarantees that $\alpha > 0$, completing the proof.

□

B. Momentum Analysis under Block Structure

B.1. Assumptions

Assumption B.1. We consider a parameter space with n blocks, where each block i contains d_i parameters. The parameter vector corresponding to block i is denoted as θ_i', where $\theta_i' \in \mathbb{R}^{d_i}$.

Assumption B.2. The block diagonal matrix of the Hessian is denoted as H_{ii}', where $i \in \{1,\ldots,n\}$. Each block H_{ii}' corresponds to the second derivative matrix for the parameters of block i, and is assumed to be positive semi-definite.

Assumption B.3. For the momentum method, we assume that the gradient $g_{t,i}$ for each block i is an independent and identically distributed (i.i.d.) random variable with mean μ_i and variance σ_i^2.

Assumption B.4. The momentum update at time step t is given by the following recurrence relation:

$$m_t = \beta m_{t-1} + (1-\beta)g_t$$

where $\beta \in (0,1)$ is the momentum coefficient, and m_t represents the momentum at time step t.

Additionally, v_t denotes the exponentially moving average of the squared gradients (second moment) for the parameter vector at time t, defined as:

$$v_t = \beta_2 v_{t-1} + (1-\beta_2)g_t^2$$

where $\beta_2 \in (0,1)$ is the decay rate, and g_t is the gradient at time step t. The term v_t plays a crucial role in scaling the learning rate and reducing the variance of parameter

B.2. Proof of Corollary 3.4

Corollary B.5. *Under the conditions specified in Assumptions B.1, B.2, B.3, and B.4, the momentum method demonstrates enhanced stability compared to the standard gradient method. Specifically, the following quantitative properties hold:*

- *The variance of parameter updates is reduced by a factor of $\frac{(1-\beta)^2}{1-\beta^2} < 1$, indicating a decrease in variance.*

- *The off-diagonal terms in the update matrix are suppressed by a factor of* $\left(\frac{(1-\beta)^2}{1-\beta^2}\right)^2$*, further reducing instability during the update.*

Here, $\beta \in (0,1)$ *is the momentum coefficient, typically in the range of 0.9 to 0.99 in practice.*

Proof. To begin, we consider a single block, denoted as block 1. The parameter vector for this block is $\theta_1' = (\theta_{1,1}, \ldots, \theta_{1,d_1})$. The block Hessian matrix H_1' is assumed to be of the form:

$$H_1' = \begin{bmatrix} H_{11} & \ldots & H_{1d_1} \\ \vdots & \ddots & \vdots \\ H_{d_1 1} & \ldots & H_{d_1 d_1} \end{bmatrix}$$

The quadratic form of the block Hessian for the parameter vector θ_1' is:

$$\theta'^{\top}_1 H_1' \theta_1' = \sum_{i=1}^{d_1} \theta_{1i}^2 H_{1i} + \sum_{i \neq j} \theta_{1i}\theta_{1j}(H_{ij} + H_{ji})$$

Extending this result to all blocks, we obtain the full expression for the directional sharpness (DS) of the parameter update under the block structure.

The momentum update at each time step t is recursively defined as:

$$m_t = (1-\beta)\sum_{i=0}^{\infty} \beta^i g_{t-i}$$

For the gradient update, the variance of the parameter update is:

$$\text{Var}(\Delta\theta_{ki}) = \frac{\eta^2 \sigma_i^2}{v_{t,i}}$$

For the momentum update, the variance of the parameter update is:

$$\begin{aligned} \text{Var}(\Delta\theta_{ki}) &= \frac{\eta^2(1-\beta)^2}{v_{t,i}} \text{Var}\left(\sum_{j=0}^{\infty} \beta^j g_{t-j,i}\right) \\ &= \frac{\eta^2(1-\beta)^2\sigma_i^2}{v_{t,i}(1-\beta^2)} \end{aligned}$$

The variance ratio between the momentum update and the gradient update is then:

$$\frac{\text{Var}(\Delta\theta_{ki})_{\text{momentum}}}{\text{Var}(\Delta\theta_{ki})_{\text{grad}}} = \frac{(1-\beta)^2}{1-\beta^2} < 1$$

The off-diagonal terms of the update matrix are proportional to the product of two parameters. Therefore, the reduction in the off-diagonal terms follows the square of the variance ratio calculated above, which is:

$$\left(\frac{(1-\beta)^2}{1-\beta^2}\right)^2$$

In the Adam optimizer, the momentum update is adjusted as follows:

$$\hat{m}_t = \frac{m_t}{1 - \beta_1^t}$$

Substituting the recursive form of m_t, we get:

$$\hat{m}_t = \frac{\beta_1 m_{t-1} + (1 - \beta_1) g_t}{1 - \beta_1^t}$$

This expression indicates that, as $t \to T$, the momentum coefficient β approaches β_1, and thus the original momentum properties hold.

Therefore, the momentum method's properties, including the reduced variance and suppressed off-diagonal terms, hold for both traditional gradient methods and the Adam optimizer with momentum correction.

□

C. Masking Strategy Analysis

Theorem C.1 (Optimality of Asynchronous Masking)**.** *Assume the following conditions:*

- *The second moment of the gradient is bounded:* $0 < \sigma_{\min}^2 \leq \mathbb{E}[g_i^2] \leq \sigma_{\max}^2$
- *The correlation between the gradient and historical momentum satisfies:* $\mathbb{E}[g_i m_{t-1,i}] = \rho_i \mathbb{E}[g_i^2]$*, where* ρ_i *is the correlation coefficient.*
- *The momentum update rule is:* $m_t = \beta_1 m_{t-1} + (1 - \beta_1) g_t$*, where* $0 < \beta_1 < 1$*.*
- *The performance metric is:* $P(A) = \alpha GC(A) - \beta DS(A)$*, where* $\alpha, \beta > 0$*.*

The asynchronous masking strategy outperforms the synchronous masking strategy.

Proof. We begin by defining key sets:

- S_1: The set of elements where the mask is 1 in the synchronous strategy, representing parameters where the momentum and gradient are aligned at the current time step.
- S_2: The set of elements where the mask is 1 in the asynchronous strategy, representing parameters where the momentum from a previous time step and the current gradient are aligned.
- S_{12}: The set of elements where the mask is 1 in both strategies ($S_1 \cap S_2$).
- S_{11}: The set of elements where the mask is 1 only in the synchronous strategy ($S_1 \setminus S_{12}$).

Let the sizes of these sets be denoted as s_1, s_2, s_{12}, and s_{11}, respectively.

For $i \in S_{12}$, from the definition we have $m_{t-1,i} g_{t,i} > 0$, so $\rho_i > 0$.

For $i \in S_{11}$, we have $-\frac{1-\beta_1}{\beta_1} g_{t,i}^2 < m_{t-1,i} g_{t,i} < 0$. This implies that $\rho_i < 0$ and $|\rho_i| < \frac{1-\beta_1}{\beta_1}$. This constraint arises from:

- If $|\rho_i| \geq \frac{1-\beta_1}{\beta_1}$, the update of m_t would lead to the gradient and momentum being aligned, which contradicts the assumption that $i \in S_{11}$.
- $\rho_i < 0$ ensures that the gradient is opposite to the historical momentum, consistent with the definition of S_{11}.

For $i \in S_{12}$, we have:

$$\mathbb{E}[g_i(\beta_1 m_{t-1,i} + (1-\beta_1)g_i)] = \beta_1 \rho_i \sigma_i^2 + (1-\beta_1)\sigma_i^2 > 0$$

To compute the difference in GC:

$$\Delta GC = (\eta_2 - \eta_1) \sum_{i \in S_{12}} g_i(\beta_1 m_{t-1,i} + (1-\beta_1)g_i) - \eta_1 \sum_{i \in S_{11}} g_i(\beta_1 m_{t-1,i} + (1-\beta_1)g_i)$$

According to the analysis in Corollary 3.4, the directional sharpness can be decomposed into diagonal and off-diagonal terms:

$$DS(A) = \sum_{k=1}^{n} {\theta'}_{kk}^{\top} H'_{kk} \theta'_{kk}$$

where H'_{kk} is the block-diagonal Hessian matrix, and θ'_{kk} is the corresponding parameter vector.

The diagonal terms can be further decomposed as:

$$\sum_{k=1}^{n} \sum_{i=1}^{d_k} \theta_{ki}^2 H_{ki} + \sum_{k=1}^{n} \sum_{i \neq j} \theta_{ki}\theta_{kj}(H_{ij} + H_{ji})$$

where the first term is the main term, and the second term is the residual.

Now, consider the difference in DS between the two strategies:

$$ds_1 = \eta_1^2 \sum_{k=1}^{n} \left(\sum_{i \in S_{11}} + \sum_{i \in S_{12}} \right) \mathbb{E}[g_i^2] + \eta_1^2 R_1$$
$$ds_2 = \eta_2^2 \sum_{k=1}^{n} \left(\sum_{i \in S_2} \right) \mathbb{E}[g_i^2] + \eta_2^2 R_2$$

where R_1 and R_2 are the residuals for each strategy.

The difference in DS can be expressed as:

$$ds_2 - ds_1 = (\eta_2^2 - \eta_1^2) \sum_{k=1}^{n} \sum_{i \in S_{12}} \mathbb{E}[g_i^2] - \eta_1^2 \sum_{k=1}^{n} \sum_{i \in S_{11}} \mathbb{E}[g_i^2] + (\eta_2^2 R_2 - \eta_1^2 R_1)$$

Assuming the learning rates are equal ($\eta_1 = \eta_2$), under expected conditions we have:

Thus, we get:

$$\mathbb{E}(\Delta GC) = \mathbb{E}\left(-\eta_1 \sum_{i \in S_{11}} g_i(\beta_1 m_{t-1,i} + (1-\beta_1)g_i) \right) = -(\beta_1 \rho_i \sigma_i^2 + (1-\beta_1)\sigma_i^2)$$

For $i \in S_{11}$, we have:

$$\mathbb{E}[g_i(\beta_1 m_{t-1,i} + (1-\beta_1)g_i)] = \beta_1 \rho_i \sigma_i^2 + (1-\beta_1)\sigma_i^2 < 0$$

This negative value arises from the fact that $\rho_i < 0$ and $|\rho_i| < \frac{1-\beta_1}{\beta_1}$.

Therefore, $\mathbb{E}(\Delta GC) > 0$, and:

$$\mathbb{E}(\Delta DS) = \mathbb{E}\left(-\eta_1^2 \sum_{k=1}^{n} \sum_{i \in S_{11}} \mathbb{E}[g_i^2] \right) < 0$$

Combining the results from the GC and DS analyses, under the conditions specified in the theorem, we obtain:

$$\Delta P = \alpha \Delta GC - \beta \Delta DS > 0$$

This completes the proof that the asynchronous masking strategy outperforms the synchronous masking strategy. □

D. Dynamic Mask Strength Analysis

Theorem D.1. *Under the following conditions: (1) The parameter space dimension d is sufficiently large. (2) The Hessian matrix H can be decomposed as $H = D + E$, where D is a diagonal matrix and E is a non-diagonal error term satisfying $\|E\|_2 \leq \varepsilon\|D\|_2$. (3) D is a positive definite matrix. (4) The learning rate $\eta > 0$,*

the following two properties hold:

Property 1 (Scaling Behavior): The first and second derivatives of the compensation factor $\alpha(t)$ with respect to the learning rate η satisfy:

$$\frac{\partial \alpha(t)}{\partial \eta} = \mathcal{O}(\|D\|_2) + \mathcal{O}(\varepsilon)$$

$$\frac{\partial^2 \alpha(t)}{\partial \eta^2} = \mathcal{O}(\|D\|_2^2) + \mathcal{O}(\varepsilon\|D\|_2^2)$$

Property 2 (Orthogonality): For any $\epsilon > 0$, with probability at least $1 - \delta$:

$$\frac{v_\eta^T v_\alpha}{\|v_\eta\|\|v_\alpha\|} \leq \varepsilon$$

where v_η and v_α denote the gradient vectors with respect to η and α, respectively.

Proof. For the parameter w_{ij}, the update u_{ij} is defined as:

$$u_{ij} = -\eta\alpha(t)\left(\beta m_{t,ij} + g_{t,ij}\right)$$

where $m_{t,ij}$ is the momentum term and $g_{t,ij}$ is the gradient term.

According to condition (2), we approximate the loss function by a second-order Taylor expansion,then we have:

$$g_{t+1} = g_t - (D + E)u_t$$

$$= g_t - \eta\alpha(t)(D + E)(\beta m_t + g_t)$$

The compensation factor $\alpha(t)$ is defined as:

$$\alpha(t) = \sqrt{\frac{\sum_{i=1}^{d} u_i^2}{\sum_{i\in S} u_i^2}}$$

where S is the selected subset of parameters.

The first derivative of $\alpha(t)$ with respect to η is:

$$\frac{\partial \alpha(t)}{\partial \eta} = \frac{1}{2\alpha(t)} \cdot \frac{\partial}{\partial \eta}\left(\frac{\sum_{i=1}^{d} u_i^2}{\sum_{i\in S} u_i^2}\right)$$

Using the chain rule and the bound $\|E\|_2 \leq \varepsilon\|D\|_2$ from condition (2), we obtain:

$$\frac{\partial \alpha(t)}{\partial \eta} = \mathcal{O}(\|D\|_2) + \mathcal{O}(\varepsilon)$$

Similarly, continuing the differentiation gives:

$$\frac{\partial^2 \alpha(t)}{\partial \eta^2} = \mathcal{O}(\|D\|_2^2) + \mathcal{O}(\varepsilon\|D\|_2^2)$$

$$v_\eta = \left[\frac{\partial u_{ij}}{\partial \eta}\right]_{i,j=1}^{d}$$

$$v_\alpha = \left[\frac{\partial u_{ij}}{\partial \alpha(t)}\right]_{i,j=1}^{d}$$

From the update rule, we know that v_η is primarily determined by:

$$v_\eta \propto -\alpha(t)(\beta m_t + g_t)$$

v_α is mainly determined by the local geometric structure:

$$v_\alpha \propto -\eta(\beta m_t + g_t)$$

In a d-dimensional parameter space, when d is large enough, by random matrix theory, for any $\epsilon > 0$:

$$P\left(\left|\frac{v_\eta^T v_\alpha}{\|v_\eta\|\|v_\alpha\|}\right| \geq \varepsilon\right) \leq 2e^{-d\varepsilon^2/2}$$

To ensure the probability is at least $1-\delta$, we need:

$$d > \frac{2\log(2/\delta)}{\varepsilon^2}$$

This completes the proof of Property 2. □

Remark D.2. 1. The $\mathcal{O}(\cdot)$ notation in the theorem implies a constant factor that is independent of the problem size. 2. The orthogonality result suggests that η and $\alpha(t)$ can be adjusted relatively independently, which is important for the stability of the optimization algorithm. 3. In practical applications, the dimension d does not need to be infinite, only sufficiently large to meet the probabilistic bound.

E. Convergence Analysis

Consider the following core algorithm steps:

$$\begin{aligned}
g_t &= \nabla \mathcal{L}(\theta_t) \\
d_t &= g_t \odot m_{t-1} \\
m_t &= \beta_1 m_{t-1} + (1-\beta_1) g_t \\
v_t &= \beta_2 v_{t-1} + (1-\beta_2)(g_t \odot g_t) \\
u_t &= \frac{m_t}{\sqrt{v_t} + \epsilon} \\
\varphi_t &= \mathbb{I}(d_t > 0) \\
\theta_{t+1} &= \theta_t - \eta \varphi_t \circ u_t
\end{aligned}$$

Along with the problem:

$$\min_{\theta \in \mathbb{R}^d} \mathcal{L}(\theta)$$

Our proof refers to the techniques in (Shi et al., 2021).

E.1. Core Lemmas

Our analysis is based on the following key property:

Lemma E.1. *For a function $f : \mathbb{R}^n \to \mathbb{R}$ with an L-Lipschitz continuous gradient, for any $x, y \in \mathbb{R}^n$, the following inequality holds:*

$$f(y) \leq f(x) + \langle \nabla f(x), y - x \rangle + \frac{L}{2}\|y - x\|^2.$$

Proof. Consider the integral along the path from x to y:

$$f(y) = f(x) + \int_0^1 \langle \nabla f(x + t(y - x)), y - x \rangle dt.$$

By the Lipschitz continuity of the gradient, we have:

$$\|\nabla f(x + t(y - x)) - \nabla f(x)\| \leq Lt\|y - x\|.$$

Thus,

$$\begin{aligned} f(y) &\leq f(x) + \langle \nabla f(x), y - x \rangle + \int_0^1 \langle \nabla f(x + t(y - x)) - \nabla f(x), y - x \rangle dt \\ &\leq f(x) + \langle \nabla f(x), y - x \rangle + \frac{L}{2}\|y - x\|^2. \end{aligned}$$

□

Lemma E.2. *For the Adam-type optimization algorithm, if $\beta_1 \leq \sqrt{\beta_2}$, in each iteration we have the bound Update the step size bound,*

$$|\theta_{i,t+1} - \theta_{i,t}| \leq \eta_t \frac{1 - \beta_1}{\sqrt{1 - \beta_2}\left(1 - \frac{\beta_1}{\sqrt{\beta_2}}\right)}$$

Proof. According to Adam update formula,

$$\begin{aligned} |\theta_{i,t+1} - \theta_{i,t}| &= \eta_t \frac{|m_{i,t}|}{\sqrt{v_{i,t}}} \\ &= \eta_t \frac{(1 - \beta_1)\sum_{s=0}^{t-1} \beta_1^s |\nabla \mathcal{L}_{i,t-s}|}{\sqrt{(1 - \beta_2)\sum_{s=0}^{t-1} \beta_2^s \nabla \mathcal{L}_{i,t-s}^2}} \\ &\overset{(\circ)}{\leq} \eta_t \sum_{s=0}^{t-1} \frac{(1 - \beta_1)\,|\nabla \mathcal{L}_{i,t-s}|}{\sqrt{(1 - \beta_2)\beta_2^s \nabla \mathcal{L}_{i,t-s}^2}} \beta_1^s \\ &= \eta_t \sum_{s=0}^{t-1} \frac{(1 - \beta_1)}{\sqrt{(1 - \beta_2)}} \left(\frac{\beta_1}{\sqrt{\beta_2}}\right)^s \\ &\overset{(*)}{\leq} \eta_t \sum_{s=0}^{+\infty} \frac{(1 - \beta_1)}{\sqrt{(1 - \beta_2)}} \left(\frac{\beta_1}{\sqrt{\beta_2}}\right)^s \\ &= \eta_t \frac{1 - \beta_1}{\sqrt{1 - \beta_2}\left(1 - \frac{\beta_1}{\sqrt{\beta_2}}\right)} \end{aligned}$$

Here, $(\circ)$ is obtained by applying the Cauchy-Schwarz inequality. $(*)$ holds trivially.

□

Lemma E.3. *We define $\Omega_t = \frac{\eta_1 L\sqrt{d}(1-\beta_1)}{\sqrt{1-\beta_2}\left(1-\frac{\beta_1}{\sqrt{\beta_2}}\right)\sqrt{t}}$, Where d is the parameter dimension. For any coordinate i, if:$|\partial_i \mathcal{L}_t| \geq \frac{4\sqrt{2}\Omega_t}{1-\beta_2}$ Then the second-moment estimation satisfies: $v_{i,t-1} \leq \frac{5}{2}|\partial_i \mathcal{L}_t|^2$*

Proof.

$$\begin{aligned}
|\nabla\mathcal{L}_{i,t} - \nabla\mathcal{L}_{i,t-s}| &\le L|\theta_{i,t} - \theta_{i,t-s}| \\
&= L|\theta_t - \theta_{t-1} + \theta_{t-1}\cdots + \theta_{t-s-1} - \theta_{t-s}| \\
&\overset{(*)}{\le} L(|\theta_t - \theta_{t-1}| + \cdots + |\theta_{t-s-1} - \theta_{t-s}|) \\
&\overset{E.2}{=} \Omega_{t-1} + \cdots + \Omega_{t-s} \\
&= \frac{\eta_1 L\sqrt{d}(1-\beta_1)}{\sqrt{1-\beta_2}\left(1-\frac{\beta_1}{\sqrt{\beta_2}}\right)} \sum_{i=t-s}^{t-1} \frac{1}{\sqrt{i}} \\
&\overset{(\circ)}{\le} \frac{\eta_1 L\sqrt{d}(1-\beta_1)}{\sqrt{1-\beta_2}\left(1-\frac{\beta_1}{\sqrt{\beta_2}}\right)} \frac{2s}{\sqrt{t-1}} \\
&= \frac{2s}{\sqrt{t-1}}\Omega_1
\end{aligned}$$

Where $(*)$is because of Triangle inequality, $(\circ)$ is because of $\sum_{p=1}^{M} \frac{1}{\sqrt{k-p}} \le \int_{k-M-1}^{k-1} \frac{dt}{\sqrt{t}} = \frac{2M}{\sqrt{k-M-1}+\sqrt{k-1}} \le \frac{2M}{\sqrt{k-1}}$.

By expanding the recurrence for the second moment, we have:

$$\begin{aligned}
v_{i,t-1} &= (1-\beta_2)\sum_{j=1}^{t-1} \left(\nabla\mathcal{L}_{i,t-j}\right)^2 \beta_2^{j-1} \\
&= (1-\beta_2)\sum_{j=1}^{t-1} \left|\nabla\mathcal{L}_{i,t-j}\right|^2 \beta_2^{j-1} \\
&\overset{(*)}{\le} (1-\beta_2)\sum_{j=1}^{t-1} \left(|\nabla\mathcal{L}_{i,t}| + \frac{2j}{\sqrt{t-1}}\Omega_1\right)^2 \beta_2^{j-1}
\end{aligned}$$

Where $(*)$is because of $|\nabla\mathcal{L}_{i,t-s}| - |\nabla\mathcal{L}_{i,t}| \le |\nabla\mathcal{L}_{i,t} - \nabla\mathcal{L}_{i,t-s}| \le \frac{2s}{\sqrt{t-1}}\Omega_1$

When $t \ge 2$,we have $\frac{2j}{\sqrt{t-1}} \le \frac{2\sqrt{2}j}{\sqrt{t}}$,so

$$\begin{aligned}
v_{i,t-1} &\le (1-\beta_2)\left(\sum_{j=1}^{t-1}\left(|\nabla\mathcal{L}_{i,t}| + \frac{2\sqrt{2}j}{\sqrt{t}}\Omega_1\right)^2 \beta_2^{j-1}\right) \\
&\le (1-\beta_2)\sum_{j=1}^{\infty}\left(|\nabla\mathcal{L}_{i,t}| + \frac{2\sqrt{2}j}{\sqrt{t}}\Omega_1\right)^2 \beta_2^{j-1} \\
&= (1-\beta_2)\sum_{j=1}^{\infty}\left(|\nabla\mathcal{L}_{i,t}|^2 \beta_2^{j-1} + \frac{4\sqrt{2}j}{\sqrt{t}}\Omega_1 |\nabla\mathcal{L}_{i,t}| \beta_2^{j-1} + \frac{8j^2\eta_1^2 dL^2}{t(1-\beta_2)}\frac{(1-\beta_1)^2}{(1-\frac{\beta_1}{\sqrt{\beta_2}})^2}\beta_2^{j-1}\right) \\
&\overset{(*)}{=} |\nabla\mathcal{L}_{i,t}|^2 + \frac{4\sqrt{2}L\eta_1\sqrt{d}L}{\sqrt{t}}\frac{1-\beta_1}{1-\frac{\beta_1}{\sqrt{\beta_2}}}|\nabla\mathcal{L}_{i,t}|\frac{1}{(1-\beta_2)^{\frac{3}{2}}} + \frac{8\eta_1^2 dL^2(1+\beta_2)}{t(1-\beta_2)^3}\frac{(1-\beta_1)^2}{(1-\frac{\beta_1}{\sqrt{\beta_2}})^2} \\
&\le |\nabla\mathcal{L}_{i,t}|^2 + |\nabla\mathcal{L}_{i,t}|\frac{4\sqrt{2}\Omega_t}{(1-\beta_2)} + \frac{16\Omega_t^2}{(1-\beta_2)^2}
\end{aligned}$$

Where $(*)$ is because of $(1-\beta_2)\sum_{j=1}^{\infty} j\beta_2^{j-1} = \frac{1}{1-\beta_2}$, $(1-\beta_2)\sum_{j=1}^{\infty} j^2\beta_2^{j-1} = \frac{1+\beta_2}{(1-\beta_2)^2}$. Then, if $|\nabla\mathcal{L}_{i,t}| \ge 4\sqrt{2}\frac{\Omega_t}{1-\beta_2}$,we have $v_{i,t-1} \le \frac{5}{2}|\nabla\mathcal{L}_{i,t}|^2$.

□

Lemma E.4. *We define* $\Omega_t = \frac{\eta_1 L\sqrt{d}(1-\beta_1)}{\sqrt{1-\beta_2}\left(1-\frac{\beta_1}{\sqrt{\beta_2}}\right)\sqrt{t}}$*, for* $t > 1$ *and* $\beta_1 < \sqrt{\beta_2}$*,we have,*

$$\left\langle \nabla\mathcal{L}_t, \eta_t \frac{-\varphi_t \circ m_t}{\sqrt{v_t}} \right\rangle \leq -\eta_t \frac{\|\nabla\mathcal{L}_t\|_\varphi}{\sqrt{10}} + \eta_t 4\sqrt{2}\frac{\Omega_1 d}{\sqrt{t}} \left(\frac{1}{1-\beta_2} + \frac{2\beta_1}{1-\beta_1}\right)\left(\frac{1}{\sqrt{10}} + \frac{1-\beta_1}{\sqrt{1-\beta_2}\left(1-\frac{\beta_1}{\sqrt{\beta_2}}\right)}\right)$$

Proof. It follows from Lemma E.3 that,

$$|\nabla\mathcal{L}_{i,t} - \nabla\mathcal{L}_{i,t-s}| \leq \frac{2s}{\sqrt{t-1}}\Omega_1$$

Multiply both sides by $|\nabla\mathcal{L}_{i,t}|$,Starting from the inequality:

$$|\nabla\mathcal{L}_{i,t} - \nabla\mathcal{L}_{i,t-s}| \cdot |\nabla\mathcal{L}_{i,t}| \leq |\nabla\mathcal{L}_{i,t}|\frac{2s}{\sqrt{t-1}}\Omega_1$$

Case 1: $\nabla\mathcal{L}_{i,t} - \nabla\mathcal{L}_{i,t-s} \geq 0$ From the above inequality:

$$\nabla\mathcal{L}_{i,t}|\nabla\mathcal{L}_{i,t}| - \nabla\mathcal{L}_{i,t-s}|\nabla\mathcal{L}_{i,t}| \leq |\nabla\mathcal{L}_{i,t}|\frac{2s}{\sqrt{t-1}}\Omega_1,$$

rearranging terms, we obtain:

$$\nabla\mathcal{L}_{i,t-s}|\nabla\mathcal{L}_{i,t}| \geq \nabla\mathcal{L}_{i,t}|\nabla\mathcal{L}_{i,t}| - |\nabla\mathcal{L}_{i,t}|\frac{2s}{\sqrt{t-1}}\Omega_1.$$

Case 1.1: If $\nabla\mathcal{L}_{i,t} > 0$ Since $|\nabla\mathcal{L}_{i,t}| = \nabla\mathcal{L}_{i,t}$, we can directly write:

$$\nabla\mathcal{L}_{i,t}\nabla\mathcal{L}_{i,t-s} \geq \nabla\mathcal{L}_{i,t}^2 - \nabla\mathcal{L}_{i,t}\frac{2s}{\sqrt{t-1}}\Omega_1.$$

Case 1.2: If $\nabla\mathcal{L}_{i,t} < 0$ Here, $|\nabla\mathcal{L}_{i,t}| = -\nabla\mathcal{L}_{i,t}$, so:

$$-\nabla\mathcal{L}_{i,t}^2 + \nabla\mathcal{L}_{i,t-s}(-\nabla\mathcal{L}_{i,t}) \leq -\nabla\mathcal{L}_{i,t}\frac{2s}{\sqrt{t-1}}\Omega_1,$$

simplifying further:

$$\nabla\mathcal{L}_{i,t-s}\nabla\mathcal{L}_{i,t} \leq \nabla\mathcal{L}_{i,t}^2 + |\nabla\mathcal{L}_{i,t}|\frac{2s}{\sqrt{t-1}}\Omega_1.$$

Case 2: $\nabla\mathcal{L}_{i,t} - \nabla\mathcal{L}_{i,t-s} \leq 0$ For this case, a similar argument applies.

Case 2.1: If $\nabla\mathcal{L}_{i,t} > 0$ The inequality directly follows as:

$$\nabla\mathcal{L}_{i,t-s}\nabla\mathcal{L}_{i,t} \leq \nabla\mathcal{L}_{i,t}^2 + |\nabla\mathcal{L}_{i,t}|\frac{2s}{\sqrt{t-1}}\Omega_1.$$

Case 2.2: If $\nabla\mathcal{L}_{i,t} < 0$ Using a similar expansion, we obtain:

$$\nabla\mathcal{L}_{i,t}\nabla\mathcal{L}_{i,t-s} \geq \nabla\mathcal{L}_{i,t}^2 - |\nabla\mathcal{L}_{i,t}|\frac{2s}{\sqrt{t-1}}\Omega_1.$$

Regardless of the sign of $\nabla\mathcal{L}_{i,t} - \nabla\mathcal{L}_{i,t-s}$, we always arrive at the following conclusion:

$$\nabla\mathcal{L}_{i,t}\nabla\mathcal{L}_{i,t-s} \geq \nabla\mathcal{L}_{i,t}^2 - |\nabla\mathcal{L}_{i,t}|\frac{2s}{\sqrt{t-1}}\Omega_1.$$

Then,we have,

$$\begin{aligned}
m_{i,t}\nabla\mathcal{L}_{i,t} &= (1-\beta_1)\sum_{s=0}^{t-1}\nabla\mathcal{L}_{i,t}\nabla\mathcal{L}_{i,t-s}\beta_1^s \\
&\geq (1-\beta_1)\sum_{s=0}^{t-1}\left(\nabla\mathcal{L}_{i,t}^2 - |\nabla\mathcal{L}_{i,t}|\frac{2s\Omega_1}{\sqrt{t-1}}\right)\beta_1^s \\
&\overset{(*)}{=} \nabla\mathcal{L}_{i,t}^2\left(1-\beta_1^t - \frac{2\Omega_1}{\sqrt{t-1}\,|\nabla\mathcal{L}_{i,t}|}\left(\frac{\beta_1}{1-\beta_1} - \beta_1^t t - \frac{\beta_1^{t+1}}{1-\beta_1}\right)\right) \\
&> \nabla\mathcal{L}_{i,t}^2\left(1-\beta_1^t - \frac{2\Omega_1}{\sqrt{t-1}\,|\nabla\mathcal{L}_{i,t}|}\frac{\beta_1}{1-\beta_1}\right).
\end{aligned}$$

where $(*)$ is because of $\sum_{k=0}^{n-1} z^k = \frac{z^n-1}{z-1}$ and $\sum_{k=0}^{n-1} kz^k = \frac{(n-1)z^{n+1}-nz^n+z}{(z-1)^2}$

Thus if $t > \max\{\log_{\beta_1}\frac{1}{4}, 1\}$ and $|\nabla\mathcal{L}_{i,t}| > \frac{8\sqrt{2}\Omega_1}{\sqrt{t}}\frac{\beta_1}{1-\beta_1}$,it reduces to:

$$m_{i,t}\nabla\mathcal{L}_{i,t} \geq \frac{\nabla\mathcal{L}_{i,t}^2}{2}$$

According to Lemma $E.3$,if $|\nabla\mathcal{L}_{i,t}| > 4\sqrt{2}\frac{\Omega_1}{\sqrt{t}}\left(\frac{1}{1-\beta_2} + \frac{2\beta_1}{1-\beta_1}\right)$, we have

$$m_{i,t}\frac{\nabla\mathcal{L}_{i,t}}{\sqrt{v_{i,t}}} \geq \frac{\nabla\mathcal{L}_{i,t}^2}{2\sqrt{v_{i,t}}} \geq \frac{\nabla\mathcal{L}_{i,t}^2}{2\sqrt{\frac{5}{2}\nabla\mathcal{L}_{i,t}^2}} = \frac{|\nabla\mathcal{L}_{i,t}|}{\sqrt{10}}$$

So we have,

$$\nabla\mathcal{L}_{i,t}\frac{m_{i,t}}{\sqrt{v_{i,t}}} \geq \frac{|\nabla\mathcal{L}_{i,t}|}{\sqrt{10}} - 4\sqrt{2}\frac{\Omega_1}{\sqrt{t}}\left(\frac{1}{1-\beta_2} + \frac{2\beta_1}{1-\beta_1}\right)\left(\frac{1}{\sqrt{10}} + \frac{1-\beta_1}{\sqrt{1-\beta_2}\left(1-\frac{\beta_1}{\sqrt{\beta_2}}\right)}\right).$$

On the contrary, if $|\nabla\mathcal{L}_{i,t}| \leq 4\sqrt{2}\frac{\Omega_1}{\sqrt{t}}\left(\frac{1}{1-\beta_2} + \frac{2\beta_1}{1-\beta_1}\right)$, According to Lemma $E.2$,we have

$$\begin{aligned}
\nabla\mathcal{L}_{i,t}\frac{m_{i,t}}{\sqrt{v_{i,t}}} &\geq -|\nabla\mathcal{L}_{i,t}|\frac{1-\beta_1}{\sqrt{1-\beta_2}\left(1-\frac{\beta_1}{\sqrt{\beta_2}}\right)} \\
&= \frac{|\nabla\mathcal{L}_{i,t}|}{\sqrt{10}} - |\nabla\mathcal{L}_{i,t}|\left(\frac{1}{\sqrt{10}} + \frac{1-\beta_1}{\sqrt{1-\beta_2}\left(1-\frac{\beta_1}{\sqrt{\beta_2}}\right)}\right) \\
&\geq \frac{|\nabla\mathcal{L}_{i,t}|}{\sqrt{10}} - 4\sqrt{2}\frac{\Omega_1}{\sqrt{t}}\left(\frac{1}{1-\beta_2} + \frac{2\beta_1}{1-\beta_1}\right)\left(\frac{1}{\sqrt{10}} + \frac{1-\beta_1}{\sqrt{1-\beta_2}\left(1-\frac{\beta_1}{\sqrt{\beta_2}}\right)}\right)
\end{aligned}$$

If is a synchronous mask, then

$$\begin{aligned}\sum_{i=1}^{d}\varphi_t\nabla\mathcal{L}_{i,t}\frac{m_{i,t}}{\sqrt{v_{i,t}}} &\geq \sum_{i=1}^{d}\nabla\mathcal{L}_{i,t}\frac{m_{i,t}}{\sqrt{v_{i,t}}} \geq \sum_{i=1}^{d}\left(\frac{|\nabla\mathcal{L}_{i,t}|}{\sqrt{10}} - 4\sqrt{2}\frac{\Omega_1}{\sqrt{t}}\left(\frac{1}{1-\beta_2}+\frac{2\beta_1}{1-\beta_1}\right)\left(\frac{1}{\sqrt{10}}+\frac{1-\beta_1}{\sqrt{1-\beta_2}\left(1-\frac{\beta_1}{\sqrt{\beta_2}}\right)}\right)\right)\\ &\geq \sum_{i=1}^{d}\left(\frac{|\nabla\mathcal{L}_{i,t}|}{\sqrt{10}} - 4\sqrt{2}\frac{\Omega_1}{\sqrt{t}}\left(\frac{1}{1-\beta_2}+\frac{2\beta_1}{1-\beta_1}\right)\left(\frac{1}{\sqrt{10}}+\frac{1-\beta_1}{\sqrt{1-\beta_2}\left(1-\frac{\beta_1}{\sqrt{\beta_2}}\right)}\right)\right)\\ &= \frac{\|\nabla\mathcal{L}_t\|_1}{\sqrt{10}} - 4\sqrt{2}\frac{\Omega_1 d}{\sqrt{t}}\left(\frac{1}{1-\beta_2}+\frac{2\beta_1}{1-\beta_1}\right)\left(\frac{1}{\sqrt{10}}+\frac{1-\beta_1}{\sqrt{1-\beta_2}\left(1-\frac{\beta_1}{\sqrt{\beta_2}}\right)}\right)\end{aligned}$$

If the mask is asynchronous, the situation is slightly more complex. According to the definition of the mask, if $\nabla\mathcal{L}_{i,t}\cdot m_{i,t-1}>0$, then $\nabla\mathcal{L}_{i,t}\cdot m_{i,t}>0$. Let the elements satisfying this condition belong to the set S_1.

If $\nabla\mathcal{L}_{i,t}\cdot m_{i,t-1}<0$, then when $\frac{m_{i,t-1}}{\nabla\mathcal{L}_{i,t}}>-\frac{1-\beta_1}{\beta_1}$, we have $\nabla\mathcal{L}_{i,t}\cdot m_{i,t}>0$. Let the elements satisfying this condition belong to the set S_2. On the other hand, when $\frac{m_{i,t-1}}{\nabla\mathcal{L}_{i,t}}<-\frac{1-\beta_1}{\beta_1}$, we have $\nabla\mathcal{L}_{i,t}\cdot m_{i,t}<0$. Let the elements satisfying this condition belong to the set S_3. And then,

$$\begin{aligned}\sum_{i=1}^{d}\varphi_t\nabla\mathcal{L}_{i,t}\frac{m_{i,t}}{\sqrt{v_{i,t}}} &= \sum_{i\in S_1}\varphi_{i,t}^{S_1}\nabla\mathcal{L}_{i,t}\frac{m_{i,t}}{\sqrt{v_{i,t}}}+\sum_{i\in S_2}\varphi_{i,t}^{S_2}\nabla\mathcal{L}_{i,t}\frac{m_{i,t}}{\sqrt{v_{i,t}}}+\sum_{i\in S_3}\varphi_{i,t}^{S_3}\nabla\mathcal{L}_{i,t}\frac{m_{i,t}}{\sqrt{v_{i,t}}}\\ &= \sum_{i\in S_1}\nabla\mathcal{L}_{i,t}\frac{m_{i,t}}{\sqrt{v_{i,t}}}\end{aligned}$$

We need to determine whether the following expression holds:

$$\sum_{i\in S_2}\nabla\mathcal{L}_{i,t}\frac{m_{i,t}}{\sqrt{v_{i,t}}}+\sum_{i\in S_3}\nabla\mathcal{L}_{i,t}\frac{m_{i,t}}{\sqrt{v_{i,t}}} = \sum_{i\in S_2}\nabla\mathcal{L}_{i,t}\frac{\beta_1 m_{i,t-1}+(1-\beta_1)\nabla\mathcal{L}_{i,t}}{\sqrt{v_{i,t}}}+\sum_{i\in S_3}\nabla\mathcal{L}_{i,t}\frac{\beta_1 m_{i,t-1}+(1-\beta_1)\nabla\mathcal{L}_{i,t}}{\sqrt{v_{i,t}}}<0$$

However, this requires additional assumptions and is quite complex. Therefore, for the asynchronous mask, we define the L_1 norm of the masked gradients affecting the update as $\sum_{i\in S_1}|\nabla\mathcal{L}_{i,t}|=\|\mathcal{L}_t\|_\varphi$.

Therefore,

$$\begin{aligned}\sum_{i=1}^{d}\varphi_t\nabla\mathcal{L}_{i,t}\frac{m_{i,t}}{\sqrt{v_{i,t}}} &\geq \sum_{i=1}^{s_1}\nabla\mathcal{L}_{i,t}\frac{m_{i,t}}{\sqrt{v_{i,t}}}\\ &\geq \sum_{i=1}^{s_1}\left(\frac{|\nabla\mathcal{L}_{i,t}|}{\sqrt{10}} - 4\sqrt{2}\frac{\Omega_1}{\sqrt{t}}\left(\frac{1}{1-\beta_2}+\frac{2\beta_1}{1-\beta_1}\right)\left(\frac{1}{\sqrt{10}}+\frac{1-\beta_1}{\sqrt{1-\beta_2}\left(1-\frac{\beta_1}{\sqrt{\beta_2}}\right)}\right)\right)\\ &= \frac{\|\nabla\mathcal{L}_t\|_\varphi}{\sqrt{10}} - 4\sqrt{2}\frac{\Omega_1 s_1}{\sqrt{t}}\left(\frac{1}{1-\beta_2}+\frac{2\beta_1}{1-\beta_1}\right)\left(\frac{1}{\sqrt{10}}+\frac{1-\beta_1}{\sqrt{1-\beta_2}\left(1-\frac{\beta_1}{\sqrt{\beta_2}}\right)}\right)\\ &> \frac{\|\nabla\mathcal{L}_t\|_\varphi}{\sqrt{10}} - 4\sqrt{2}\frac{\Omega_1 \arg\min\{s_1^t\}}{\sqrt{t}}\left(\frac{1}{1-\beta_2}+\frac{2\beta_1}{1-\beta_1}\right)\left(\frac{1}{\sqrt{10}}+\frac{1-\beta_1}{\sqrt{1-\beta_2}\left(1-\frac{\beta_1}{\sqrt{\beta_2}}\right)}\right)\end{aligned}$$

Let $s_0=\arg\min s_1^t\leq d$ in the iteration from t to T, So we have

$$\left\langle \nabla\mathcal{L}_t, \eta_t \frac{-\varphi_t \circ m_t}{\sqrt{v_t}} \right\rangle \leq -\eta_t \frac{\|\nabla\mathcal{L}_t\|_\varphi}{\sqrt{10}} + \eta_t 4\sqrt{2}\frac{\Omega_1 s_0}{\sqrt{t}} \left(\frac{1}{1-\beta_2} + \frac{2\beta_1}{1-\beta_1}\right)\left(\frac{1}{\sqrt{10}} + \frac{1-\beta_1}{\sqrt{1-\beta_2}\left(1-\frac{\beta_1}{\sqrt{\beta_2}}\right)}\right)$$
$$\leq -\eta_t \frac{\|\nabla\mathcal{L}_t\|_\varphi}{\sqrt{10}} + \eta_t 4\sqrt{2}\frac{\Omega_1 d}{\sqrt{t}} \left(\frac{1}{1-\beta_2} + \frac{2\beta_1}{1-\beta_1}\right)\left(\frac{1}{\sqrt{10}} + \frac{1-\beta_1}{\sqrt{1-\beta_2}\left(1-\frac{\beta_1}{\sqrt{\beta_2}}\right)}\right)$$

□

E.2. Proof of Theorem 3.8

Theorem E.5. *For the full-batch AlphaAdam algorithm, assuming that Assumptions3.7 hold, and $\beta_1 < \sqrt{\beta_2} < 1$ with the step size $\eta_t = \frac{\eta}{\sqrt{t}}$, the following holds:*

$$\min_{t\in(1,T]} \|\nabla\mathcal{L}_t\|_\varphi \leq \mathcal{O}\left(\frac{\log T}{\sqrt{T}}\right)$$

Proof. First, apply the Lemma E.1 as follows,

$$\mathcal{L}(\theta_{t+1}) - \mathcal{L}(\theta_t) \leq \langle \nabla\mathcal{L}(\theta_t), \theta_{t+1} - \theta_t\rangle + \frac{L}{2}\|\theta_{t+1} - \theta_t\|^2$$
$$\leq \left(-\eta_t \left\langle \nabla\mathcal{L}_t, \frac{\varphi_t \circ m_t}{\sqrt{\beta_2 v_{t-1} + (1-\beta_2)\nabla\mathcal{L}_t^2}} \right\rangle + \frac{L}{2}\eta_t^2 \frac{d}{1-\beta_2}\frac{(1-\beta_1)^2}{(1-\frac{\beta_1}{\sqrt{\beta_2}})^2}\right)$$

Let $M_1 = 4\sqrt{2}\Omega_1 d\left(\frac{1}{1-\beta_2} + \frac{2\beta_1}{1-\beta_1}\right)\left(\frac{1}{\sqrt{10}} + \frac{1-\beta_1}{\sqrt{1-\beta_2}\left(1-\frac{\beta_1}{\sqrt{\beta_2}}\right)}\right)$,$M_2 = \eta_1^2 \frac{Ld}{2(1-\beta_2)}\frac{(1-\beta_1)^2}{(1-\frac{\beta_1}{\sqrt{\beta_2}})^2}$.

Sum the inequality from t_0 to T, and using the lower bound of the objective function $\mathcal{L}^\star$ and Lemma E.4, we obtain:

$$\mathcal{L}(\theta_{T+1}) - \mathcal{L}(\theta_{t_0}) \leq -\sum_{t=t_0}^{T} \frac{\eta_1}{\sqrt{t}} \left\langle \nabla\mathcal{L}_t, \frac{\varphi_t \circ m_t}{\sqrt{\beta_2 v_{t-1} + (1-\beta_2)\nabla\mathcal{L}_t^2}} \right\rangle + \sum_{t=t_0}^{T} \eta_1^2 \frac{1}{t}\frac{Ld}{2(1-\beta_2)}\frac{(1-\beta_1)^2}{(1-\frac{\beta_1}{\sqrt{\beta_2}})^2}$$
$$\leq \sum_{t=t_0}^{T}\left(-\eta_t \frac{\|\nabla\mathcal{L}_t\|_\varphi}{\sqrt{10}} + \frac{M_1}{t}\right) + \sum_{t=t_0}^{T}\frac{M_2}{t}$$

Rearrange the above inequality,

$$\sum_{t=t_0}^{T} \frac{\|\nabla\mathcal{L}_t\|_\varphi}{\sqrt{t}\sqrt{10}} \leq \sum_{t=t_0}^{T} \frac{M_2 + M_1}{t} + \mathcal{L}(\theta_{t_0}) - \mathcal{L}(\theta_{T+1})$$

Because of $\sum_{t=t_0}^{T}\frac{1}{t} \leq \int_{t_0}^{T+1}\frac{1}{x}dx = \log\frac{T+1}{t_0}$ and $\sum_{t=t_0}^{T}\frac{1}{\sqrt{t}} \geq 2\left(\sqrt{T} - \sqrt{t_0 - 1}\right)$. So we have,

$$\|\nabla\mathcal{L}_t\|_\varphi \leq \frac{\sqrt{10}}{2}\frac{\left(\log\frac{T+1}{t_0}(M_1+M_2) + \mathcal{L}(\theta_{t_0}) - \mathcal{L}(\theta_{T+1})\right)}{(\sqrt{T} - \sqrt{t_0 - 1})}$$

So we prove that,

$$\min_{t\in(1,T]} \|\nabla\mathcal{L}_t\|_\varphi \leq \mathcal{O}\left(\frac{\log T}{\sqrt{T}}\right)$$

□

F. More Eperimental Details

F.1. Fine-Tuning on GLUE

We fine-tune the pre-trained RoBERTa-Base model(Liu et al., 2019b) on the GLUE benchmark using the Hugging Face implementation[1][2]. For all tasks except QQP, we employ a batch size of 32, while QQP uses a larger batch size of 128 due to its dataset characteristics. The model is trained uniformly for 3 epochs across all tasks with a weight decay of 0.01 and a maximum sequence length of 512. For each task, we perform a grid search over learning rates in the range of $\{1\text{e-}5, 2\text{e-}5, 3\text{e-}5, 4\text{e-}5, 5\text{e-}5\}$ and report the average of the best results. The complete hyperparameter configurations are summarized in Table 6. For AlphaAdam, Adam, Adam-mini, and CAdam, we use $\beta_1 = 0.9$ and $\beta_2 = 0.999$. For LDAdam and Galore, we use $\beta_1 = 0.9$ and $\beta_2 = 0.99$.

Training Samples	MRPC	STS-B	CoLA	RTE	SST-2	QNLI	QQP
Batch Size	32	32	32	32	32	32	128
Epochs				3			
Weight Decay				0.01			
Max Seq Len				512			

Table 4. Hyperparameters used for fine-tuning on GLUE.

F.2. Pretraining on OpenWebText

We utilize the nanoGPT codebase[3] to pretrain GPT-2 models (Radford et al., 2019) (Small, Medium, and Large) on the OpenWebText dataset[4]. The hyperparameter configurations are detailed in Table 5. The models span a parameter range from 125M to 770M, with corresponding increases in hidden size, number of attention heads, and number of transformer layers. We perform learning rate tuning over the set $\{6\text{e-}4, 3\text{e-}4, 2\text{e-}4\}$, and employ the following optimizer settings: weight decay coefficient $\lambda = 0.1$, $\epsilon = 1\text{e-}8$, $\beta_1 = 0.9$, and $\beta_2 = 0.95$. To ensure stable and efficient pretraining, we set batch sizes to 12, 6, and 4 for the Small, Medium, and Large models, respectively.

Model	Size	d_model	n_head	depth	learning rate	batch size
Small	125M	768	12	12	6e-4	12
Medium	355M	1024	16	24	3e-4	6
Large	770M	1280	20	36	2e-4	4

Table 5. Hyperparameters used for training models of different sizes.

F.3. Fine-Tuing on GSM8K

We fine-tune the pre-trained Llama2-7B model (Touvron et al., 2023) using the llm-foundry codebase[5] with evaluation via standardized lm-evaluation-harness[6] on the GSM8K benchmark with the Hugging Face implementation[7]. The fine-tuning process employs consistent hyperparameters across all optimizers, including AlphaAdam, Adam-8bit, Decoupled AdamW, and CAdamW. Specifically, we train for 3 epochs with a total of 702 training steps, including 20 warm-up steps. The batch size is set to 32, and the maximum sequence length is 512. We use a learning rate of 5e-5 and optimizer parameters $\beta_1 = 0.9$ and $\beta_2 = 0.999$. The complete hyperparameter configurations are summarized in Table 6.

F.4. Alpha Value During Training

We conducted a detailed analysis of the alpha values for all trainable parameters in both the Llama 2 7B model and GPT-2 Small during training, presenting the specific alpha values for each parameter as shown in Figures 4 and 5. The Llama 2 7B

[1] https://huggingface.co/transformers/model_doc/roberta.html
[2] https://huggingface.co/datasets/nyu-mll/glue
[3] https://github.com/karpathy/nanoGPT/tree/master
[4] https://huggingface.co/datasets/Skylion007/openwebtext
[5] https://github.com/hiyouga/LLaMA-Factory
[6] https://github.com/EleutherAI/lm-evaluation-harness
[7] https://huggingface.co/datasets/openai/gsm8k

Table 6. Hyperparameter configurations for fine-tuning Llama2-7B on GSM8K.

Hyperparameter	**Value**
Epochs	3
Training Steps	702
Warm-up Steps	20
Batch Size	32
Maximum Length	512
Learning Rate	5e-5
β_1	0.9
β_2	0.999

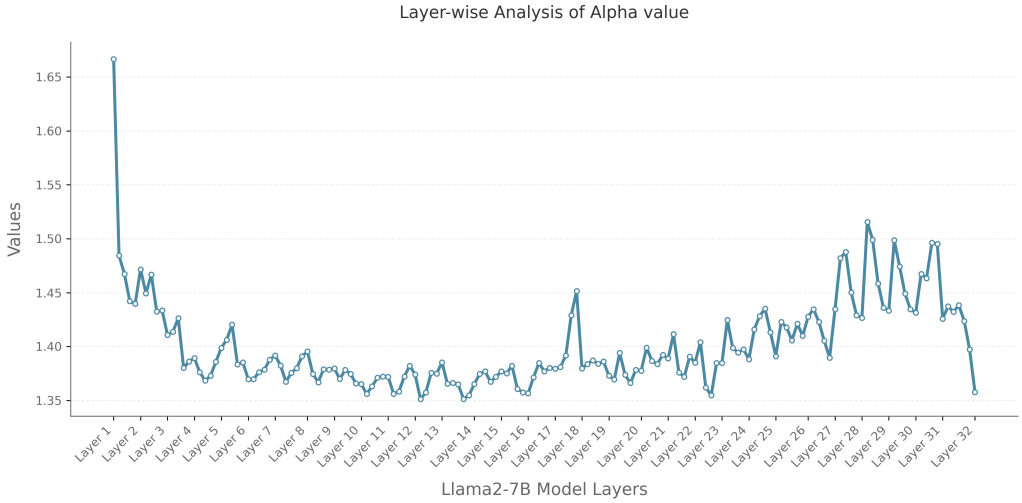

Figure 4. Randomly selected alpha value distribution for all layers in a single step of training in the Llama2-7B model.

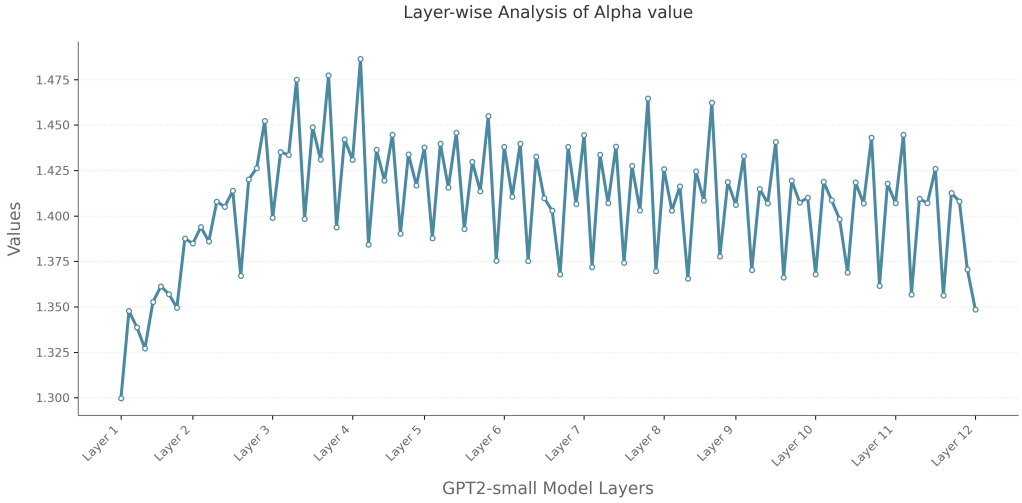

Figure 5. Randomly selected alpha value distribution for all layers in a single step of training in the GPT2-125M model.

model consists of 161 parameter groups, while GPT-2 Small contains 108 parameter groups. Throughout the training, the distribution of alpha values remained stable, with $\alpha_{\max}$ set to 2 in our implementation.